



## A time like our own? Radioisotopic calibration of the Ordovician greenhouse to icehouse transition

M. Elliot Smith <sup>a,\*</sup>, Brad S. Singer <sup>b</sup>, Toni Simo <sup>c</sup>

<sup>a</sup> Department of Geology, Sonoma State University, 1801 E Cotati Ave, Rohnert Park, CA 94928, United States

<sup>b</sup> Department of Geoscience, University of Wisconsin, 1215 W. Dayton St., Madison, WI 53706, United States

<sup>c</sup> ExxonMobil, Upstream Research, P.O. Box 2189, Houston, TX 77252-2189, United States

### ARTICLE INFO

#### Article history:

Received 16 May 2011

Received in revised form 6 September 2011

Accepted 8 September 2011

Available online xxxx

Editor: T.M. Harrison

#### Keywords:

Ordovician

<sup>40</sup>Ar/<sup>39</sup>Ar

U–Pb

$\delta^{13}\text{C}$

timescale

tiered interpolation

### ABSTRACT

Tiered interpolation, a new timescale methodology, was used to construct the first radioisotopically-calibrated composite  $\delta^{13}\text{C}$  curve for the Ordovician period using sanidine <sup>40</sup>Ar/<sup>39</sup>Ar age determinations and existing U–Pb geochronology and biostratigraphic zonation. Tiered interpolation intercalates and temporally scales the numerical age of lithostratigraphic horizons by conducting a series of nested projections between hierarchical temporal control points. For primary control points, new <sup>40</sup>Ar/<sup>39</sup>Ar ages and legacy U–Pb geochronology were screened to avoid analyses affected by inheritance and daughter loss and calibrated to reflect modern decay constants and standard values. Ages for secondary, tertiary, etc.... control points are obtained via linear interpolation of between higher order control points. In scaling the Ordovician  $\delta^{13}\text{C}$  composite, the following control point order was applied: (1) radioisotopic ages (2) graptolite Zones, (3) index taxa-based on speciation events (North Atlantic conodont Zones), (4) North American Mid-continent conodont zones, and (5) stratal thicknesses at  $\delta^{13}\text{C}$  sampled sections. The resulting timescale utilizes the highest resolution of each component, is internally consistent, and is re-scalable as more precise radioisotopic ages become available. It provides a robust framework for independently assessing the accuracy of biostratigraphic composite timescales because it does not rely an assumption of quasi-continuous sediment accumulation and/or speciation. To better calibrate the Late Ordovician and resolve a discrepancy between U–Pb and <sup>40</sup>Ar/<sup>39</sup>Ar ages, three new <sup>40</sup>Ar/<sup>39</sup>Ar ages were determined via the laser fusion of multiple single sanidine phenocrysts from three bentonitic ash beds from the Late Ordovician marine strata of the upper Mississippi valley where the record of Taconic volcanism is most complete. Fusions of 275 individual sanidine crystals from the Millbrig, Dygerts, and Rifle Hill bentonites yield largely Gaussian apparent age distributions with a small number of readily identified outliers and stratigraphically-consistent weighted mean ages of  $454.1 \pm 1.4$  Ma (51 of 57),  $450.7 \pm 1.4$  Ma (39 of 74), and  $450.3 \pm 1.9$  Ma (96 of 144) for the Millbrig, Dygerts, and Rifle Hill bentonites, respectively ( $2\sigma$  analytical uncertainties relative to 28.201 Ma for FCs). The Millbrig age is consistent with the existing U–Pb ages for both the underlying Deicke bentonite and the Kinnekulle bentonite of Sweden. The new age model permits the assembly of the first complete radioisotopically-calibrated composite  $\delta^{13}\text{C}$  curve for the Ordovician, the first icehouse to occur subsequent to the Cambrian explosion. The resulting  $\delta^{13}\text{C}$  composite integrates all available graptolite and conodont biostratigraphic with radioisotopic ages and indicates that previous biostratigraphic composites incorporate  $2\sigma$  errors up to ~5 Ma. When viewed without temporal distortions, isotopic carbon excursions (ICEs) in the Ordovician appear to have occurred at a similar tempo as ICEs in the better resolved Cenozoic greenhouse to icehouse transition. Although boundary conditions for oceanography, biogeography, and continental configuration are strikingly different, the tempo of isotopic changes, growth of south-polar ice sheets, and concurrent oceanic and geomorphic responses bears both similarities and differences with the better understood Cenozoic era.

© 2011 Elsevier B.V. All rights reserved.

### 1. Introduction

The Ordovician period (493–443 Ma) and Cenozoic era (66–0 Ma) both were times of south-polar continental ice sheet growth on a

previously ice-free Earth which corresponded to major reorganizations of biotic, oceanographic, and landscape processes (Frakes et al., 1992). Icehouse conditions at the end of the Ordovician culminated in a large positive carbon isotope excursion, and the second largest mass extinction in Earth history (Berry et al., 2002; Sepkoski, 1995). The progression of events in both the Ordovician and Cenozoic periods are recorded by positive isotopic carbon ( $\delta^{13}\text{C}$ ) excursions (ICEs) (Saltzman, 2005; Zachos et al., 2001) that have been attributed to both enhancement

\* Corresponding author.

E-mail address: [michael.smith@sonoma.edu](mailto:michael.smith@sonoma.edu) (M.E. Smith).

of thermohaline ocean circulation and upwelling-driven sequestration of  $\delta^{13}\text{C}$ -depleted organic matter (Patzkowsky et al., 1997), and to eustatically-driven exposure and weathering of  $^{13}\text{C}$ -enriched carbonate platforms (Kump et al., 1999). However, direct comparison of the tempo and magnitude of climatic events of the Ordovician with the much better-resolved Cenozoic (Zachos et al., 2001) has been hampered by contradictory radioisotopic dating, uncertain calibration of the U–Pb and  $^{40}\text{Ar}/^{39}\text{Ar}$  chronometers, and stratigraphic uncertainties (Renne et al., 1998; Sadler and Cooper, 2004). Here we use a tiered interpolation of conodont and graptolite biostratigraphic zonation between  $^{40}\text{Ar}/^{39}\text{Ar}$  and U–Pb age determinations for ash beds to construct a radioisotopically-based age model for the Ordovician period. To augment Late Ordovician geochronology and resolve the discrepancy between previously published geochronology (Min et al., 2001; Renne et al., 2010; Tucker and McKerrow, 1995), three new  $^{40}\text{Ar}/^{39}\text{Ar}$  ages were determined for three bentonitic ash beds from North America via the laser fusion of multiple single sanidine phenocrysts. The resulting timescale is used to independently assess the accuracy of the timescales used to construct previous  $\delta^{13}\text{C}$  composites (Bergström et al., 2009; Saltzman, 2005; Young et al., 2009, 2010), and to numerically calibrate a new composite  $\delta^{13}\text{C}$  curve for the Ordovician period with the least temporal distortion currently possible (Fig. 1).

## 2. Ordovician K-bentonites

Bentonitic ash horizons were selected for geochronology from the Late Ordovician marine strata of the upper Mississippi valley (UMV) where the record of Taconic volcanism is most complete (Kolata et al., 1996). Initially a mixture of fine glass and volcanic phenocrysts, these beds were converted to K-bentonites via alteration of glass ash to montmorillonite clay minerals and orthoclase (Hay et al., 1988), partly due to fluids responsible for Mississippi Valley type mineralization (Rowan and Goldhaber, 1995). Correlations based on phenocryst chemistry indicate that UMV K-bentonites constitute the thin (<10 cm) distal edges of enormous ash deposits that blanketed eastern Laurentia and central Baltoscandia, reaching >1 m thickness in Appalachia and Sweden (Huff et al., 2010; Kolata et al., 1996, 1998). The Millbrig bentonite (Willman and Kolata, 1978) and Kinnekulle bentonite bed in Baltoscandia (Bergström et al., 1995) are both composite beds with multiple fall-out layers, contain similar phenocrysts, and occur in bio- and chemo-stratigraphically similar horizons, and are hypothesized to have been erupted from a similar series of eruptions (Bergström et al., 2004; Huff et al., 1992, 2010; Saltzman et al., 2003), however, their correlation is inconsistent with the biotite  $^{40}\text{Ar}/^{39}\text{Ar}$  age determinations of Min et al. (2001). The Millbrig, or I-2 bentonite (Mossler and Hayes, 1966) was sampled from the Glencoe Member of the Spechts Ferry Formation near Decorah, Iowa (IA). The lowermost of the ashes studied for this report, the Millbrig defines the Turinian–Chatfieldian Stage boundary within the North American Mohawkian Series (Leslie and Bergström, 2005; Sweet, 1995), has been correlated across the eastern U.S.A. (Haynes, 1994; Kolata et al., 1996; Mitchell et al., 2004), and occurs ~1 m above the Deicke bentonite. The Dygerts (Willman and Kolata, 1978) or I-7 (Mossler and Hayes, 1966) bentonite was collected from its type section near Galena, Illinois (IL) where it occurs in the Sinsinawa Member of the Wise Lake Formation of the Galena Group (Willman and Kolata, 1978) and can be traced from IL to Minnesota (MN). Finally, the Rifle Hill bentonite (Kolata et al., 1996) was sampled at the Rifle Hill quarry near Chatfield, Minnesota where it occurs ~5 m above the base of the Elgin Member of the Maquoketa Formation, which conformably overlies the Galena Group.

## 3. Stratigraphy and biostratigraphy

The Galena Group and underlying Ansell Group (Templeton and Willman, 1963; Willman and Kolata, 1978) have been quantitatively sampled for conodont fossils and are overlain by the shale-rich

Maquoketa Formation that has yielded both conodonts and graptolites. In order to most precisely constrain the biostratigraphy of  $^{40}\text{Ar}/^{39}\text{Ar}$ -dated Ordovician strata in the UMV, a new correlation between northeast IL and southeast MN was constructed using published lithostratigraphy (see Table 3), apatite phenocryst chemistry of ash beds (Emerson et al., 2004), and  $\delta^{13}\text{C}$  chemostratigraphy (Fanton and Holmden, 2007; Ludvigson et al., 2004; Simo et al., 2003). Fig. 2 shows the Galena Group grading from northwest IL to southeast MN from finely-bedded bioclastic carbonates to finely intercalated carbonates, siliciclastic mudstones, and marls, suggesting marine sedimentation across a broad shelf with a flux of siliciclastic material from the north. Conodonts collected from the Spechts Ferry Formation (IA & IL), correlative Decorah Shale (MN) (Leslie, 2000; Sweet, 1987; Votaw, 1971; Webers, 1966), and underlying Glenwood and Platteville Formations (Sweet, 1987; Thompson, 1959) place the Millbrig bentonite within the upper *Amorphognathus tvaerensis* North Atlantic (NAtl) conodont Zone (*Baltoniodus alobatus* subzone) and the upper part of the *Phragmodus undatus* North American Midcontinent (NAM) conodont zone (Leslie and Bergström, 2005). Differing published biostratigraphic interpretations necessitate further examination of the strata containing the Dygerts and overlying Rifle Hill bentonites. Bergström (1971) first cited the occurrence of *Amorphognathus ordovicicus* in the Dubuque Member at Rifle Hill, MN (*Amorphognathus ordovicica* of Webers (1966)) and in Winneshiek County, IA (*Goniodontus superbus* of Ethington, 1959), placing the upper Dubuque Member in the eponymous NAtl conodont Zone (Sweet and Bergström, 1971). However, Sweet (1987) projected the base of the *Oulodus velicuspis* NAM conodont zone into the uppermost Dubuque Member, based in part on the absence *Oulodus robustus* and *Oulodus velicuspis* in collections by Webers (1966) at Rifle Hill, MN. Sweet's (1987) graphic correlation-based projection contradicts Bergström (1971) because *Amorphognathus ordovicicus* occurs within the *Aphelognathus grandis* NAM conodont zone in the most complete North American successions of this interval (Bergström et al., 2010a; Sweet, 1979a). Following Goldman and Bergström (1997), we project the *Oulodus robustus* and *Aphelognathus grandis* NAM conodont zones into the Galena Formation (Fig. 2), which is consistent with the position of the *Amplexograptus mantoulinensis*–*Dicellograptus complanatus* North American graptolite Zone boundary in the Maquoketa Formation (Goldman and Bergström, 1997). The absence of *Oulodus velicuspis*, *Oulodus robustus*, or *A. grandis* in the intervening upper Cummingsville and Prosser Members are attributed to either (a) the absence of these taxa in local faunas at Rifle Hill, or (b) stratal lacuna(e) between the first occurrence of *Belodina confluens* and the base of the Stewartville Member. In support of the latter hypothesis, the potentially lacunae-containing interval of the Prosser and Dunleith Formation was interpreted Choi et al. (1999) to include the G1–G2 sequence boundary, which has sandstone at its base (Witzke and Ludvigson, 2005), and contains siliciclastic horizons with Proterozoic-aged detrital feldspar (Chetel et al., 2005). In summary, the Dygerts and Rifle Hill bentonites straddle the *Amorphognathus superbus*–*Amorphognathus ordovicicus* NAtl conodont Zone boundary, and are projected to occur within the *Oulodus robustus* and *Aphelognathus grandis* NAM conodont zones, respectively.

## 4. $^{40}\text{Ar}/^{39}\text{Ar}$ geochronology

Sanidine crystals were isolated from K-bentonites via crushing, decanting, and sieving, and concentrated via Franz isodynamic magnetic separator, then selected under refractive index oil using a petrographic microscope. After co-irradiation with Fish Canyon tuff sanidine (FCs), individually sanidine crystals were fused using a  $\text{CO}_2$  laser and analyzed in a MAP-215 spectrometer at the University of Wisconsin Rare Gas Laboratory (see Supplementary Table S1 for complete analytical results). Fusions of 275 individual sanidine crystals from the Millbrig, Dygerts, and Rifle Hill bentonites yield largely Gaussian apparent age distributions with a small number of readily identified outliers (Fig. 3). A subset



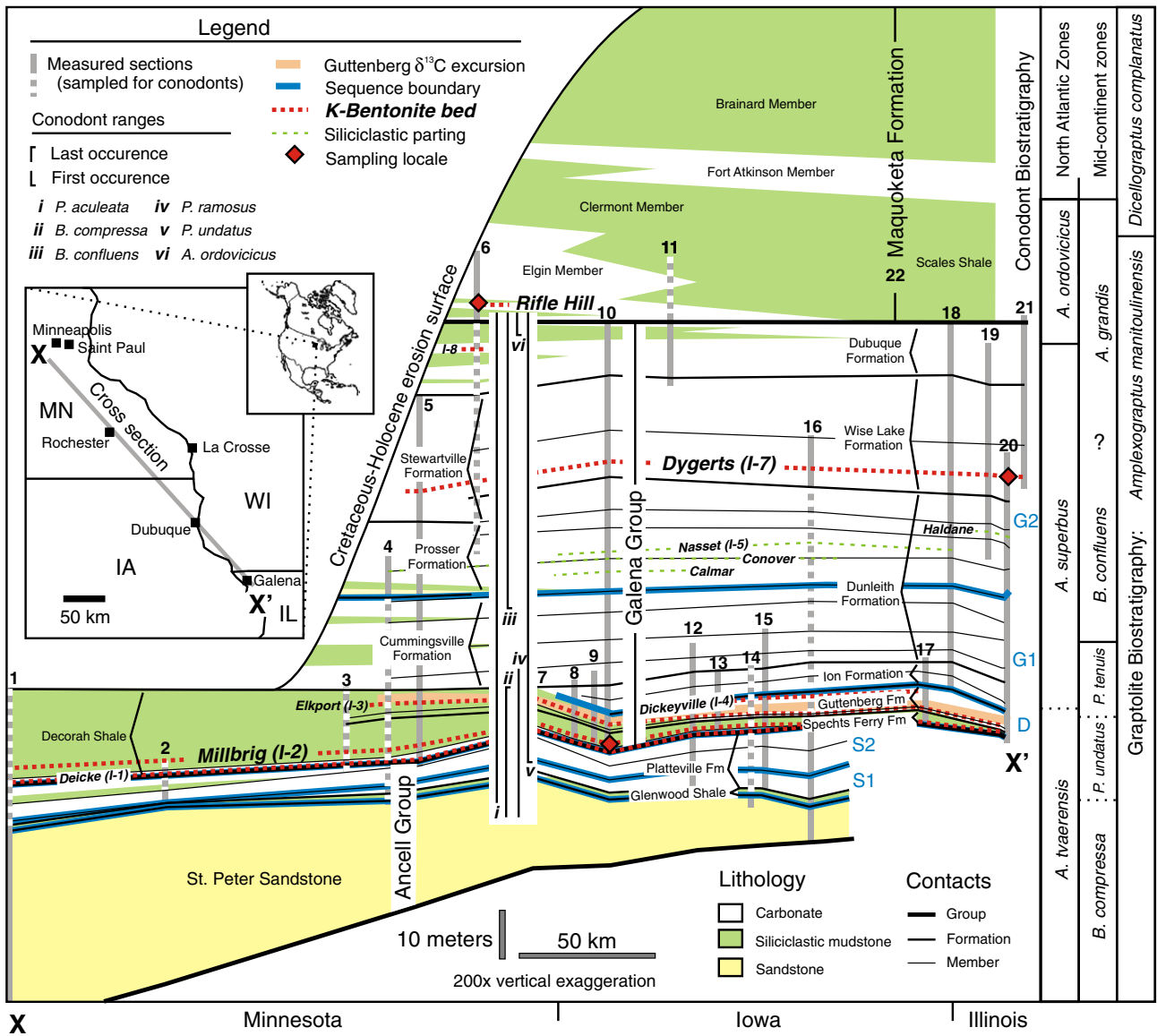


**Fig. 2.** Cross section of Upper Ordovician strata from SE Minnesota to NW Illinois showing ash beds (K-bentonites), biostratigraphy, and sequence stratigraphy (Choi and Simo, 1998; Choi et al., 1999). See Supplementary Table S3 for stratigraphic and biostratigraphic references for numbered sections, and Supplementary Table S4 for conodont genus abbreviations. Note that the recently recognized *Belodina compressa*–*Belodina confluens* speciation event (Richardson and Bergström, 2003), occurs at level Rh-24 of Webers' (1966) Rifle Hill section.

calculations, where  $f$  = the number of analyses (Wendt and Carl, 1991). As a consequence, four younger apparent ages between 418 and 438 Ma were excluded from the Millbrig population, and 8 younger apparent ages between 130 and 428 Ma and one older apparent age ( $527 \pm 7$  Ma) were excluded from the Dygerts population. Due to the very fine (60–120 mm) grain size of sanidine from the Rifle Hill bentonite, small  $^{40}\text{Ar}^*$  yields limit analytical precision for individual fusions to  $\sim \pm 4\%$ , making clear identification of outliers within 40 Ma of the mean difficult. In order to avoid subjective exclusion from either end of the distribution, a more inclusive  $\text{MSWD} > 1.5$  criteria was applied for excluding discordant apparent ages from the Rifle Hill weighted mean. Of 126 of 144 analyses not excluded based on  $^{40}\text{Ar}^*$  criteria, Rifle Hill bentonite sanidine yielded 5 younger outliers between 256 and 426 Ma and 26 older outliers. Older outliers have apparent ages ranging from 473 to 2175 Ma, similar to  $^{40}\text{Ar}/^{39}\text{Ar}$  age distributions observed in feldspar from siliciclastic horizons of the Galena Group (Fig. 2, Chetel et al., 2005) and suggestive of post eruptive incorporation of detrital feldspar.

After  $^{40}\text{Ar}^*$  filtering and MSWD-based outlier exclusion, sanidine fusions give stratigraphically-consistent weighted mean ages of  $451.5 \pm 1.3$  Ma (51 of 57,  $\text{MSWD} = 1.2$ ),  $448.3 \pm 1.4$  Ma (39 of 74,  $\text{MSWD} = 1.2$ ),  $447.9 \pm 1.8$  Ma (96 of 144,  $\text{MSWD} = 1.5$ ) for the Millbrig, Dygerts, and Rifle Hill bentonites, respectively ( $2\sigma$  analytical uncertainties relative to 28.02 Ma for FCs (Renne et al., 1998) and the  $^{40}\text{K}$  decay constants of Steiger and Jäger (1977)). The sanidine age for the Millbrig bentonite differs slightly from single-crystal biotite laser incremental heating  $^{40}\text{Ar}/^{39}\text{Ar}$  age determinations of Min et al. (2001) for Ordovician bentonite beds (Figs. 2 and 3). It is distinguishably older than its biotite age of  $448.0 \pm 2.0$  Ma (3 of 10 concordant age spectra), and indistinguishable but stratigraphically inconsistent with the biotite  $449.8 \pm 2.3$  Ma age (9 of 11 concordant age spectra) for the underlying Deicke bentonite. These apparent age discordances may reflect the greater susceptibility of biotite relative to sanidine to alteration-derived loss  $^{40}\text{Ar}^*$  (Smith et al., 2008). Interestingly, due to its older age, the sanidine age for the Millbrig overlaps with the biotite age for the Kinnekulle bentonite of Sweden, widely viewed to be its

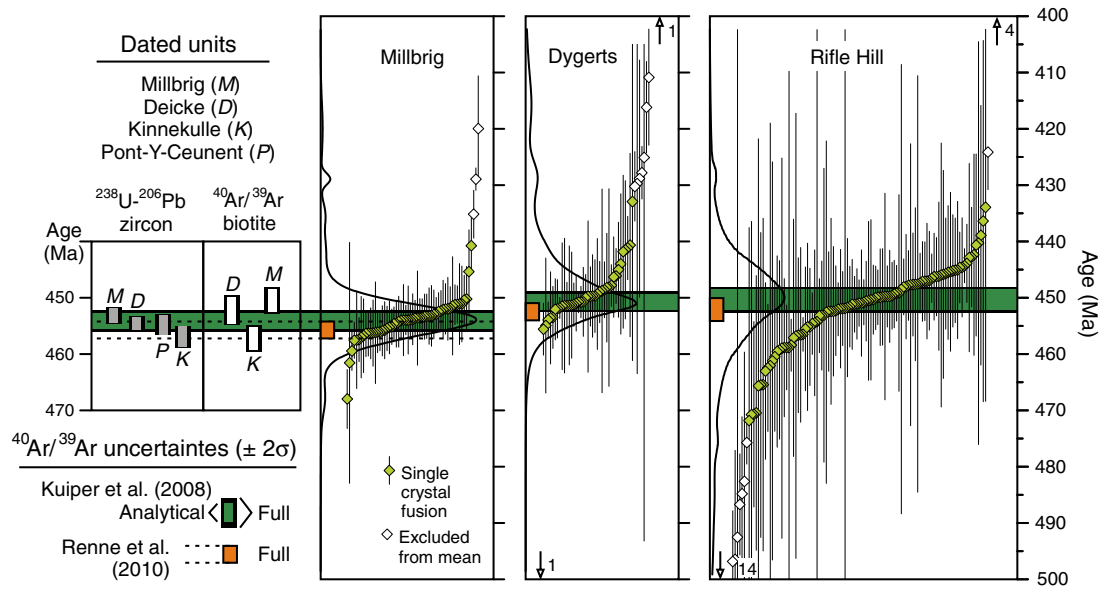


**Fig. 3.** Cumulative probability diagrams showing sanidine  $^{40}\text{Ar}/^{39}\text{Ar}$  ages for Ordovician K-bentonites ( $^{40}\text{Ar}^* > 96\%$ -screened), previously determined biotite  $^{40}\text{Ar}/^{39}\text{Ar}$  ages (Min et al., 2001) for the Millbrig, Deicke and Kinnekulle bentonites, and zircon  $^{238}\text{U}$ - $^{206}\text{Pb}$  ages for the Millbrig, Deicke and Kinnekulle bentonites, and Pont-y-ceunant ash (Renne et al., 2010; Tucker and McKerrow, 1995). Numbered open arrows indicate additional excluded analyses outside depicted temporal range. See text for detail of exclusion criteria. Gray boxes depict full zircon  $^{238}\text{U}$ - $^{206}\text{Pb}$  age uncertainties calculated following Shoene et al. (2006).

correlative (Bergström et al., 2004; Huff et al., 1992, 2010; Saltzman et al., 2003).

## 5. Radioisotopic intercalibration

Despite significant improvements to analytical precision, systematic uncertainty in the  $^{40}\text{K}$  decay constant and K/Ar-based primary standard age have until recently limited the  $2\sigma$  precision of Ordovician  $^{40}\text{Ar}/^{39}\text{Ar}$  ages to  $\pm 7$  Ma (Renne et al., 1998), precluding meaningful comparisons with U–Pb ages. Recent liquid scintillation counting measurements of  $^{40}\text{K}$  decay (Renne et al., 2010) and two independent calibrations of the  $^{40}\text{Ar}/^{39}\text{Ar}$  chronometer: via (1) co-irradiation of FCs with sanidine from ash beds within astrochronologically-dated strata of the Miocene Melilla Basin of Morocco (Kuiper et al., 2008) and (2) optimization using pairs of  $^{40}\text{Ar}/^{39}\text{Ar}$  and  $^{238}\text{U}$ - $^{206}\text{Pb}$  ages from a suite of rocks spanning Earth history (Renne et al., 2010), have reduced these systematic uncertainties from  $\sim 1.5\%$  to  $< 0.1\%$ . However, stratigraphic uncertainties intrinsic to astronomical calibration of the  $^{40}\text{Ar}/^{39}\text{Ar}$  chronometer have yet to be elucidated and may be underestimated if lacunae are present in the Melilla record, and uncertainty in calibration of the U–Pb chronometer (Schoene et al., 2006) may affect the accuracy of the optimization calculation. Nonetheless, both calibrations yield statistically indistinguishable Ordovician  $^{40}\text{Ar}/^{39}\text{Ar}$  ages that are an order of magnitude more precise than the previous

calibration (Renne et al., 1998) and consistent with CA-TIMS-based U–Pb ages (Fig. 3). Relative to the widely used 28.02 Ma age for FCs (Renne et al., 1998), these calibrations result in increases of 2.4 Ma (Kuiper et al., 2008) and 4.0 Ma (Renne et al., 2010) for late Ordovician  $^{40}\text{Ar}/^{39}\text{Ar}$  ages (Table 1, Fig. 3). The greater accuracy afforded by sanidine and both new calibrations is illustrated by the elimination of the discordance between the  $^{40}\text{Ar}/^{39}\text{Ar}$  age for the Millbrig bentonite and zircon  $^{238}\text{U}$ - $^{206}\text{Pb}$  ages for the Millbrig and Kinnekulle bentonites (Fig. 3). Although the optimization method of Renne et al. (2010) is independent of astrochronology and accounts for branched decay of  $^{40}\text{K}$ , the decision to utilize the Kuiper et al. (2008) calibration for the tiered interpolation-based age model and  $\delta^{13}\text{C}$  composite was aimed towards avoiding discordance between the sanidine  $^{40}\text{Ar}/^{39}\text{Ar}$  age for the Millbrig bentonite relative to the biotite  $^{40}\text{Ar}/^{39}\text{Ar}$  age for the Deicke bentonite (Min et al., 2001) used in the Ordovician  $^{40}\text{Ar}/^{39}\text{Ar}$ -U–Pb data pair used for the optimization calibration (Fig. 3). If optimization-calibrated  $^{40}\text{Ar}/^{39}\text{Ar}$  ages are used in the Ordovician tiered interpolation, the result is a much-shortened uppermost Sanbian (Gi2 substage, *Phragmodus undatus* NATI conodont Zone) and a 30% increase in the duration of the Upper Katian (Bo1–Bo3 substages; *Amorphognathus ordovicicus* NATI conodont Zone), but little modification to the overall trend and tempo of the  $\delta^{13}\text{C}$  events.

Both  $^{40}\text{Ar}/^{39}\text{Ar}$  and U–Pb ages are subject to subtle inheritance and daughter-loss, particularly if multi-crystal aliquots are analyzed. To

**Table 1**  
 $^{40}\text{Ar}/^{39}\text{Ar}$  ages and uncertainties.

Bentonite	Calibration:		Renne et al. (1998) <sup>a</sup>			Kuiper et al. (2008) <sup>b</sup>			Renne et al. (2010) <sup>c</sup>		
	n <sup>d</sup>	MSWD	Apparent age (Ma)	$\pm 2\sigma^e$	$\pm 2\sigma^f$	Apparent age (Ma)	$\pm 2\sigma^e$	$\pm 2\sigma^f$	Apparent age (Ma)	$\pm 2\sigma^e$	$\pm 2\sigma^f$
Millbrig	50 of 57	1.17	451.67	$\pm 1.40$	$\pm 7.09$	454.12	$\pm 1.41$	$\pm 1.89$	455.72	$\pm 1.41$	$\pm 1.50$
Dygerts	39 of 74	1.23	448.30	$\pm 1.36$	$\pm 7.04$	450.74	$\pm 1.37$	$\pm 1.86$	452.34	$\pm 1.37$	$\pm 1.47$
Rifle Hill	96 of 144	1.50	447.89	$\pm 1.84$	$\pm 7.14$	450.32	$\pm 1.85$	$\pm 2.24$	451.92	$\pm 1.85$	$\pm 1.93$

<sup>a</sup> Calculated using age and uncertainty equations and GA-1550 biotite standard values of Renne et al. (1998) relative to the decay constant values of Steiger and Jäger (1977).

<sup>b</sup> Calculated using age and uncertainty equations of Kuiper et al. (2008) and Renne et al. (1998), astrochronologically-determined 6.5 Ma primary standard age for the Melilla ash (Kuiper et al., 2008), and liquid scintillation counting-updated total decay constant value of Renne et al. (2010).

<sup>c</sup> Calculated using the Monte Carlo optimization approach of Renne et al. (2010).

<sup>d</sup> See Supplementary Table S1 for further analytical details.

<sup>e</sup> Analytical uncertainty only, when MSWD > 1, analytical uncertainty is multiplied by  $\sqrt{\text{MSWD}}$ .

<sup>f</sup> Fully propagated uncertainties, which include analytical, intercalibration, primary standard, and  $^{40}\text{K}$  decay constant uncertainties.

avoid these sources of bias, single zircon crystals are ideally annealed and chemical abraded prior to dissolution and thermal ionization mass spectrometry (CA-TIMS, Mattinson, 2005) and single sanidine crystals are screened to exclude low  $^{40}\text{Ar}^*$  analyses. However, existing U–Pb ages for several important horizons of the Ordovician were obtained prior to the advent of CA-TIMS using multi-crystal aliquots. In addition, due to the more precise constraints on the  $^{238}\text{U}$  versus  $^{235}\text{U}$  decay constants, systematic uncertainties for  $^{238}\text{U}$ – $^{206}\text{Pb}$  ages are significantly smaller than  $^{235}\text{U}$ – $^{207}\text{Pb}$  ages (Schoene et al., 2006). Consequently, radioisotopic ages used in Fig. 1 were selected according to the following order of preference: (1) single crystal  $^{238}\text{U}$ – $^{206}\text{Pb}$  CA-TIMS ages and daughter-loss screened  $^{40}\text{Ar}/^{39}\text{Ar}$  ages, (2) single crystal  $^{238}\text{U}$ – $^{206}\text{Pb}$  TIMS ages, (3) multi-crystal  $^{238}\text{U}$ – $^{206}\text{Pb}$  ages, and (4) multi-crystal  $^{235}\text{U}$ – $^{207}\text{Pb}$  ages (Table 2).

## 6. Tiered interpolation-based Age model and $\delta^{13}\text{C}$ composite

Precise relative chronologies have been developed for the Ordovician period based on graptolite and conodont fossils using graphic correlation and related computational methods (Sadler et al., 2009; Sweet, 2005). However, these chronologies individually are of limited utility in the scaling  $\delta^{13}\text{C}$  records for several geochronologic reasons. First, a subset of legacy U–Pb and  $^{40}\text{Ar}/^{39}\text{Ar}$  geochronology for the Ordovician bears evidence for inaccuracy due to miscalibration, inheritance or daughter loss. In order to mute the effect of resulting age scatter on the continuity of zone ages, recent timescale compilations (Sadler and Cooper, 2004; Sadler et al., 2009) are temporally scaled by calculating a best fit line through all available geochronology and its biostratigraphic position in the composite (Fig. 4). While useful for reducing the impact of spurious radioisotopic ages, this method also reduces the ability of geochronology to resolve secular trends in faunal origination or sedimentation rate because they are inherently assumed to be quasi-continuous by all methods of biostratigraphic compositing. Finally, graptolite faunas are often absent in the carbonate-rich strata that have provided the majority of the most detailed carbon isotopic

records and thus of limited utility to scaling the  $\delta^{13}\text{C}$  composite. However, conodont faunas are present in many of these strata, and can be related to a parallel graphical composite (Sweet, 1984, 1995, 2005).

A scaling methodology modified from Kaufmann (2006) was used to integrate graptolite and conodont biostratigraphy with radioisotopic ages that temporally arranges  $\delta^{13}\text{C}$  analyses between a series of hierarchically-nested control points (Fig. 4). Similar to the approach used by Cande and Kent (1992) to calculate Cenozoic paleomagnetic reversal ages, tiered interpolation (TI) uses radioisotopic ages as primary control points ( $c_1$ ), and calculates numerical ages for secondary, tertiary, and quaternary control point ( $c_{2-4}$ ) via interpolation of between higher order control points. In order of preference, we employ (1) graptolite Zones (Sadler et al., 2009), (2) conodont index taxa based on speciation events (North Atlantic conodont Zones) (Bergström, 1971), (3) first and last occurrences defining North American Midcontinent conodont zones of Sweet (1984, 1995, 2005), and (4) stratal thicknesses in  $\delta^{13}\text{C}$ -sampled sections (see Table 3), to scale the composite  $\delta^{13}\text{C}$  curve. Graptolite zonation is preferable to conodonts for second order calibration points because A) the majority of U–Pb-dated Ordovician volcanic units occur within graptolite bearing strata of the British Isles (Fortey et al., 2000; Tucker et al., 1990), and B) the database of graptolites-bearing shales is significantly more complete than the carbonate-based conodont composite (see caption for Fig. 5). It should be noted that biostratigraphic resolution provided by conodont zonation was used heavily in the model to scale the carbonate-based  $\delta^{13}\text{C}$  composite between graptolite Zone boundaries. The numerical age for a particular stratal position  $p_u$  is calculated by conducting a series of nested projections between hierarchically arranged control points (Fig. 4). The age of any projected position ( $p_u$ ) between two higher-level control points ( $p_1$  and  $p_2$  of ages  $t_1$  and  $t_2$ ) is:  $t_u = \frac{(p_u - p_1)(t_2 - t_1)}{p_2 - p_1} + t_1$ , in which value for  $p_u$  is expressed as a percent of the difference between  $p_1$  and  $p_2$ . The resulting timescale utilizes the highest resolution of each component, is internally consistent, and is re-scalable as more precise radioisotopic ages become available. By explicitly leveraging all available constraints to provide temporal scaling

**Table 2**  
Radioisotopic temporal control points.

Abbr. (Fig. 1)	Unit	Dated material	Type	Age (Ma)	2 $\sigma$ (analytical)	2 $\sigma$ (full) <sup>a</sup>	Reference(s)
Og	Ogof-ddú ash	4 of 9 multi-crystal aliquots of zircon	$^{238}\text{U}$ – $^{206}\text{Pb}$	490.7	±0.7	±1.1	(Davidek et al., 1998)
D	Volcaniclastic sandstone in Dol-cyn-afon Formation	4 of 22 single detrital zircon	$^{238}\text{U}$ – $^{206}\text{Pb}$ <sup>b</sup>	486.2	±1.0	±1.3	(Landing et al., 2000)
CB	Cape Breton Island bentonite	2 of 8 multi-crystal aliquots of zircon	$^{238}\text{U}$ – $^{206}\text{Pb}$ <sup>b</sup>	480.2	±2.1	±2.2	(Landing et al., 1997)
SG	Sleive Gallion rhyolite	3 of 4 single zircon (CA-TIMS)	$^{238}\text{U}$ – $^{206}\text{Pb}$	473.0	±1.8	±2.0	(Cooper et al., 2008)
2	Serw Formation ash-flow tuff	2 of 3 multi-crystal aliquots of zircon	$^{238}\text{U}$ – $^{206}\text{Pb}$ <sup>b</sup>	465.6	±0.9	±1.2	(Tucker et al., 1990)
1	Upper Lower rhyolitic tuff member: Llanrian Volc. Fm.	3 of 4 multi-crystal aliquots of zircon	$^{238}\text{U}$ – $^{206}\text{Pb}$ <sup>b</sup>	462.9	±0.9	±1.2	(Tucker and McKerrow, 1995)
15	“Calcareous” ash at Llandrindod Wells	5 of 5 multi-crystal aliquots of zircon	$^{207}\text{Pb}$ – $^{206}\text{Pb}$	460.4	±2.2	±5.1	(Tucker, 1991; Tucker and McKerrow, 1995)
De	Deicke bentonite	10 of 16 single zircon (CA-TIMS)	$^{238}\text{U}$ – $^{206}\text{Pb}$	454.6	±1.1	±1.4	(Renne et al., 2010)
M	Millbrig bentonite	50 of 57 laser fusions of single sanidine	$^{40}\text{Ar}/^{39}\text{Ar}$	455.1	±1.4	±1.7	This study
Dy	Dygers bentonite	39 of 74 laser fusions of single sanidine	$^{40}\text{Ar}/^{39}\text{Ar}$	451.6	±1.4	±1.7	This study
RH	Rifle Hill bentonite	96 of 144 laser fusions of single sanidine	$^{40}\text{Ar}/^{39}\text{Ar}$	451.2	±1.9	±2.1	This study
5	Anceps ash	4 of 9 multi-crystal aliquots of zircon	$^{238}\text{U}$ – $^{206}\text{Pb}$	444.9	±1.0	±1.2	(Tucker et al., 1990), recalculated by Compston (2000)
6	Lower Birkhill shale bentonite	6 of 8 multi-crystal aliquots of zircon	$^{238}\text{U}$ – $^{206}\text{Pb}$	439.6	±1.0	±1.2	(Tucker et al., 1990), recalculated by Compston (2000)
Os	Osmundsberg bentonite	Single zircon (CA-TIMS)	$^{238}\text{U}$ – $^{206}\text{Pb}$	438.7	±1.0	±1.2	(Bergström et al., 2008)

<sup>a</sup> Full  $^{40}\text{Ar}/^{39}\text{Ar}$  uncertainties calculated according to  $\text{FCs} = 28.201$  Ma, using the equations of Kuiper et al. (2008) and Renne et al. (1998), and liquid scintillation counting-derived decay constant values of Renne et al. (2010); full U–Pb uncertainties calculated according to Schoene et al. (2006).

<sup>b</sup> Recalculated from primary isotopic data; ages represent weighted means of youngest concordant zircon population.

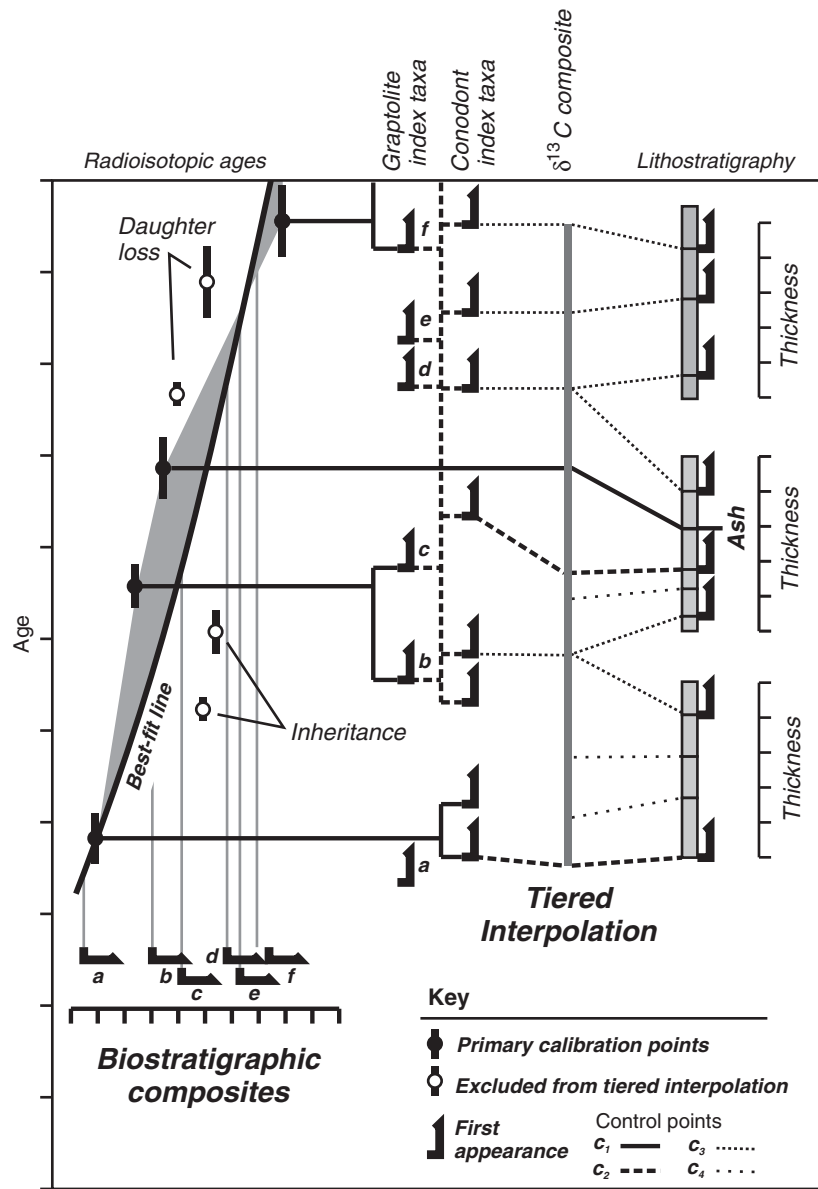


**Fig. 4.** Comparison of tiered interpolation methodology used for this study and best-fit technique used for the GTS04 (Cooper and Sadler, 2004) and CONUP (Sadler et al., 2009) timescales. Note that the calibration point hierarchy for a specific strata horizons are situationally dependent upon immediate biostratigraphic constraints. Shaded area indicates resulting offset between tiered interpolation and best-fit approaches.

for the  $\delta^{13}\text{C}$  composite, the *TI* method also provides a robust framework for propagating full age uncertainties within the resulting composite. The uncertainty in the age for any  $p_u$  can be determined by quadratic propagation of (a) full geochronologic uncertainties of the nearest radioisotopic ages and (b) the uncertainties in the position of the dated

horizon among secondary and lower level control point used to compute the age.

**Table 3**  
Tiered interpolation model ages for segments of the  $\delta^{13}\text{C}$  composite and references.

Segment	Start (Ma)	End (Ma)	Location	Reference
1	490.700	462.534	Argentina	Buggisch et al. (2003)
2	462.534	461.461	Baltoscandinavia	Schmitz et al. (2010)
3	461.357	455.078	Nevada	Saltzman and Young (2005)
4	455.078	454.155	Iowa	Ludvigson et al. (2004)
5	454.155	451.656	Kentucky	Bergström et al. (2010b)
6	451.656	451.091	Oklahoma	Bergström et al. (2010b)
7	451.091	445.854	Ohio	Bergström et al. (2010b)
8	445.854	443.004	Nevada	Saltzman and Young (2005)

Note: Numbered segments are shown under the column Strata in Fig. 1. See Supplementary Table S4 for *TI* ages of conodont and graptolite index taxa.

## 7. Comparison with previous biostratigraphic composites

The *TI* timescale permits independent evaluation of the temporal linearity of previous conodont and graptolite composites. When cross plotted, the most recent overestimate apparent age durations in the strata and paleontology-rich Sauk and Tippecanoe North American sequences of Sloss (1963), and underestimate Middle Ordovician apparent age durations (Fig. 5). The age divergence is most pronounced in the conodont composite of Sweet (2005), which is offset by as much as 6 Ma from the *TI* composite, but is clearly present (4 Ma of offset) in the global graptolite composite of Sadler et al. (2009). Given that typical  $2\sigma$  radioisotopic uncertainties are  $\pm 2$  Ma, these residuals are significant, and attest to the fundamental temporal non-linearity of the inputs to any purely biostratigraphic composite: sediment accumulation and species origination and

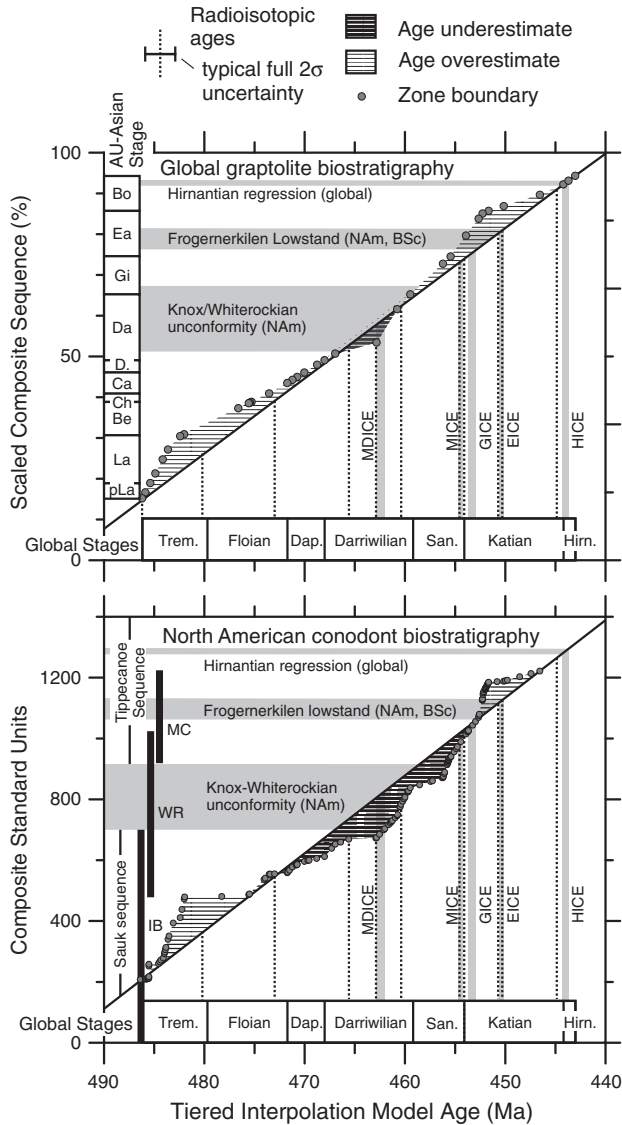


**Fig. 5.** Graphical comparison of the tiered interpolation timescale against graptolite and conodont composite timescales, illustrating eustatic and isotopic events and systemic errors. See Supplementary Table S4 for *T<sub>i</sub>* ages for graptolite and conodont zones. Plotted are ICEs (see Fig. 1 for abbreviations), 1st order sequences (Sloss, 1963), and significant eustatic events: the Himantian regression (Schmitz and Bergström, 2007), Frogemerkilen lowstand (Nielsen, 2004), and Knox-Whiterockian unconformity (Mussman and Read, 1986; Sloss, 1963; Templeton and Willman, 1963). NAM and BSc refer to North America and Baltoscandia, respectively. Graptolite biostratigraphic composite sequence was derived by Sadler et al. (2009) using the *Conup9* constrained optimization program to integrate stratal thickness and FAs and LAs of over 1900 graptolite species at over 400 individual sections worldwide, and is plotted alongside global and Australasian Stages (Webby et al., 1991, 2004). Conodont biostratigraphy was determined from the North American composite sequence of W.C. Sweet (1984, 1995, 2005) which is based on graphic correlation of North American strata to three graphically-linked regional composites: the Ibexian (IB), based on 13 localities in UT, NV, and TX (Sweet and Tolbert, 1997); Whiterockian (WR), based on 6 localities in Nevada (Sweet et al., 2005); and Mohawkian-Cincinnatian (MC) composite of 124 localities in the central United States (Sweet, 1979b, 1984, 1995).

extinction. Elimination of these errors permits a less distorted view of the isotopic events of the Ordovician.

### 8. $\delta^{13}\text{C}$ excursions and $^{87}\text{Sr}/^{86}\text{Sr}$ trends

During both the Ordovician and Cenozoic, ~25 Ma of relatively invariant  $\delta^{13}\text{C}$  was succeeded by a ~20 Ma evolution towards icehouse conditions punctuated by abrupt positive isotopic carbon excursions (ICEs) that (Fig. 1). Although the typical magnitude of an ICE is ~3 times greater during the Ordovician (2–6‰) than during the Cenozoic

(Fig. 1C), their similarly paced supraorbital macrostratigraphic (0.5 to 5 Ma) fluctuations may reflect similar Ordovician and Cenozoic responses and feedbacks between oceanic, weathering, glacial processes and the global carbon cycle to the motion of plates across the polar regions (Frakes et al., 1992). The advent of ICEs in both periods is roughly coincident with secular shifts in  $^{87}\text{Sr}/^{86}\text{Sr}$  (Qing et al., 1998; Shields et al., 2003; Young et al., 2009) and evidence for south-polar glaciation of Gondwanaland and Antarctica, respectively (Crowell, 1999; Frakes et al., 1992; Ghienne, 2003) (Fig. 1). Of the five named Ordovician ICEs, the Guttenberg (GICE, Bergström et al., 2010a; Hatch et al., 1987; Jacobson et al., 1995) and Hirnantian (HICE, Fan et al., 2009; Marshall and Middleton, 1990; Schmitz and Bergström, 2007) are best documented, while the mid-Darriwilian (MDICE, Kaljo et al., 2007; Schmitz et al., 2010), Mifflin (MICE, Ludvigson et al., 2004) and Elkhorn (EICE, Bergström et al., 2010) are less well constrained. Beginning at ~453.7 Ma, the GICE coincided with deposition of upwelling-driven phosphatic shale and ooids (Kolata et al., 2001; Pope and Steffen, 2003) and a drop in brachiopod diversity (Patzkowsky and Holland, 1997). The HICE, beginning ~444.4 Ma, coincided with a major global unconformity, ice-marginal deposits in West Africa (Ghienne, 2003), and the second largest mass extinction in Earth history (Berry et al., 2002). Similarly, the Oe-1 and Mi-1 Cenozoic ICEs have been correlated to unconformities (Haq et al., 1987), glaciation of Antarctica (Miller et al., 1991; Paul et al., 2000), and major reorganizations of biota (Zachos et al., 2001). In contrast, a prominent positive  $\delta^{13}\text{C}$  shift occurs at 16 Ma coincides with the mid-Miocene climatic optimum (MMCO) and the subsequent glaciation of East Antarctica at ca. 13 Ma was not accompanied by a positive ICE but instead coincided with a return to low  $\delta^{13}\text{C}$  values.

### 9. Discussion

There is growing consensus based on climate modeling and  $^{87}\text{Sr}/^{86}\text{Sr}$  analyses that both the Ordovician and Cenozoic icehouses were triggered by a  $p\text{CO}_2$  drawdown resulting from increased silicate weathering of nascent low latitude orogenies. In the Ordovician  $p\text{CO}_2$  drawdown appears to have been accomplished via weathering of the juvenile Taconic arc (Buggisch et al., 2010; Young et al., 2009) which would have driven down oceanic  $^{87}\text{Sr}/^{86}\text{Sr}$  values (Fig. 1), whereas weathering of the rising Himalaya and Tibetan Plateau resulted in more radiogenic oceanic  $^{87}\text{Sr}/^{86}\text{Sr}$  values in the last 20 Ma (Raymo et al., 1988). Although Cenozoic ICEs have been linked to increased ocean fertility and organic carbon burial resulting from glacially-driven upwelling (Salamy and Zachos, 1999), consensus has yet to be achieved regarding the mechanism(s) responsible for Ordovician ICEs. Two models have been proposed: (1) enhanced weathering of  $^{13}\text{C}$ -rich carbonate platforms via high  $p\text{CO}_2$  (due to decreased chemical weathering under ice sheets) & lowered sea levels. (Fantón and Holmden, 2007; Kump et al., 1999; Young et al., 2010); and (2) enhanced organic productivity and burial of isotopically light carbon resulting from thermohaline circulation following a period of stratified oligotrophic oceans with warm saline deep waters (Brenchley et al., 1994; Brenchley et al., 1995; Patzkowsky et al., 1997). Expanding upon the upwelling-driven productivity hypothesis, Saltzman (2005) proposed three hypothetical oceanic modes to explain macrostratigraphic patterns in Paleozoic  $\delta^{13}\text{C}$  proxy data: (1)  $\text{N}_2$ -limited productivity (anoxic-euxinic deep ocean, warm climate, no ICE), (2) cool P-limitation (oscillating oxic, anoxic ocean, cool climate, ICE), and (3) cold P-limitation (oxic ocean, icehouse, no ICE). Following Saltzman (2005), Ordovician ICEs would represent episodes of cool, ventilated oceans with P-limited productivity, consistent with a 1.5‰ positive excursion in  $\delta^{15}\text{N}$  during the HICE (LaPorte et al., 2009). The short-lived Hirnantian Earth thus never achieved full icehouse conditions characteristic of the glaciation of East Antarctica at ~13 Ma (Fig. 1), Carboniferous and Plio-Pleistocene glaciations (Saltzman, 2005; Zachos et al., 2001).

Supplementary materials related to this article can be found online at doi: [10.1016/j.epsl.2011.09.014](https://doi.org/10.1016/j.epsl.2011.09.014).

## Acknowledgments

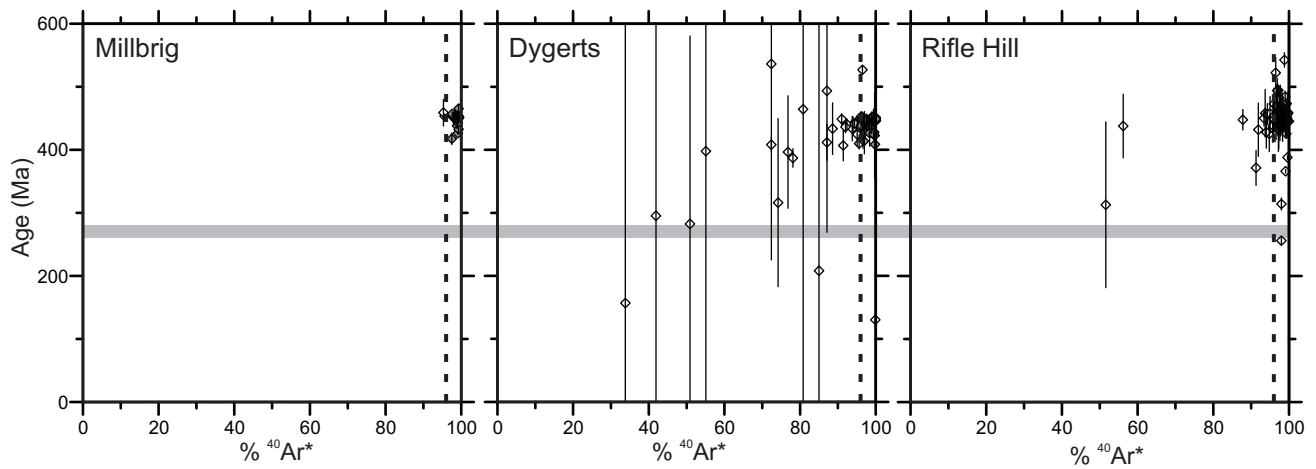
We appreciate the assistance of Brian Jicha, Clint Cowan, Lauren Chetel, Elizabeth Clechenko, Steve Beyer, and Rebecca Best, and the careful suggestions of two anonymous reviewers. This study was supported by US NSF grants EAR-0230123 and EAR-0516760 to Singer.

## References

- Bergström, S.M., Toprak, F.Ö., Huff, W.D., Mundil, R., 2008. Implications of a new, biostratigraphically well-controlled, radio-isotopic age for the lower Telychian Stage of the Llandovery Series (Lower Silurian, Sweden). *Episodes* 31, 309–314.
- Bergström, S.M., 1971. Conodont biostratigraphy of the Middle and Upper Ordovician of Europe and eastern North America. In: Sweet, W.C., Bergström, S.M. (Eds.), *Symposium on Conodont Biostratigraphy*. Memoir 127, Geological Society of America, pp. 83–161.
- Bergström, S.M., Huff, W.D., Kolata, D.R., Bauert, H., 1995. Nomenclature, stratigraphy, chemical fingerprinting, and areal distribution of some Middle Ordovician K-bentonites in Baltoscandia. *GFF* 117, 1–13.
- Bergström, S.M., Huff, W.D., Saltzman, M.R., Kolata, D.R., Leslie, S.A., 2004. The greatest volcanic ash falls in the Phanerozoic. *Sed. Rec.* 2, 4–8.
- Bergström, S.M., Chen, X., Gutierrez-Marco, J.C., Dronov, A., 2009. The new chronostratigraphic classification of the Ordovician System and its relations to major regional series and stages and to  $\delta^{13}\text{C}$  chemostratigraphy. *Lethaia* 42, 97–107.
- Bergström, S.M., Young, S., Schmitz, B., 2010a. Katian (Upper Ordovician)  $\delta^{13}\text{C}$  chemostratigraphy and sequence stratigraphy in the United States and Baltoscandia: a regional comparison. *Palaeogeogr. Palaeoclimatol. Palaeoecol.* 296, 217–234.
- Bergström, S.M., Schmitz, B., Saltzman, M.R., Huff, W.D., 2010b. The Upper Ordovician Guttenberg  $\delta^{13}\text{C}$  excursion (GICE) in North America and Baltoscandia: occurrence, chronostratigraphic significance, and paleoenvironmental relationships. In: Finney, S.C., Berry, W.B.N. (Eds.), *The Ordovician Earth System*. Special Paper 466, Geological Society of America, pp. 37–67.
- Bergström, S.M., Young, S., Schmitz, B., 2010. Katian (Upper Ordovician)  $\delta^{13}\text{C}$  chemostratigraphy and sequence stratigraphy in the United States and Baltoscandia: a regional comparison. *Palaeogeogr. Palaeoclimatol. Palaeoecol.*
- Berry, W.B.N., Ripperdan, R.L., Finney, S.C., 2002. Late Ordovician extinction: a Laurentian view. In: Koeberl, C., MacLeod, K.G. (Eds.), *Catastrophic Events and Mass Extinctions: Impacts and Beyond*. Special Paper 356, Geological Society of America, pp. 463–471.
- Brand, U., Tazawa, J., Sano, H., Azmy, K., Lee, X., 2009. Is mid-late Paleozoic ocean-water chemistry coupled with epeiric seawater isotope records? *Geology* 37, 23–26.
- Brenchley, P.J., Marshall, J.D., Carden, G.A.F., Robertson, D.B.R., Long, D.G.F., Meidla, T., Hints, L., Anderson, T.F., 1994. Bathymetric and isotopic evidence for a short-lived Late Ordovician glaciation in a greenhouse period. *Geology* 22, 295–298.
- Brenchley, P.J., Carden, G.A.F., Marshall, J.D., 1995. Environmental changes associated with the 'First Strike' of the Late Ordovician mass extinction. *Mod. Geol.* 20, 69–82.
- Bristow, T.F., Kennedy, M.J., 2008. Carbon isotope excursions and the oxidant budget of the Ediacaran atmosphere and ocean. *Geology* 36, 863–866.
- Buggisch, W., Keller, M., Lehnert, O., 2003. Carbon isotope record of Late Cambrian to Early Ordovician carbonates of the Argentine Precordillera. *Palaeogeogr. Palaeoclimatol. Palaeoecol.* 195, 357–373.
- Buggisch, W., Joachimski, M.M., Lehnert, O., Bergström, S.M., Repetski, J.E., Webers, G.F., 2010. Did intense volcanism trigger the first Late Ordovician icehouse? *Geology* 38, 327–330.
- Cande, S.C., Kent, D.V., 1992. A new geomagnetic polarity timescale for the Late Cretaceous and Cenozoic. *J. Geophys. Res.* 100, 13917–13951.
- Chetel, L.M., Simo, J.A.T., Singer, B.S., 2005.  $^{40}\text{Ar}/^{39}\text{Ar}$  geochronology and provenance of detrital K-feldspars, Ordovician, Upper Mississippi Valley. *Sediment. Geol.* 182, 163–181.
- Choi, Y.S., Simo, J.A., 1998. Ramp facies and sequence stratigraphic models in an epeiric sea: the Upper Ordovician mixed carbonate–siliclastic Glenwood and Platteville Formations, Wisconsin, USA. In: Wright, V.P., Burchette, T.P. (Eds.), *Carbonate Ramps*. Special Publication 149, The Geological Society, London, pp. 437–456.
- Choi, Y.S., Simo, J.A., Saylor, B.Z., 1999. Sedimentologic and sequence stratigraphic interpretation of mixed carbonate–siliclastic ramp, mid-continent epeiric sea, middle to upper Ordovician Decorah and Galena Formations, Wisconsin. In: Harris, P.M., Saller, A.H., Simo, J.A. (Eds.), *Carbonate Sequence Stratigraphy: Applications to Reservoirs, Outcrops and Models*. Special Publication 63, SEPM (Society for Sedimentary Geology), pp. 275–289.
- Compston, W., 2000. Interpretation of SHRIMP and isotope dilution zircon ages for the Palaeozoic time-scale: II. Silurian to Devonian. *Mineral. Mag.* 64, 1127–1146.
- Cooper, J.D., Sadler, P.M., 2004. The Ordovician period. In: Gradstein, F.M., Ogg, J.G., Smith, A.G. (Eds.), *A Geologic Time Scale 2004*. Cambridge University Press, Cambridge, pp. 165–187.
- Cooper, R.A., Crowley, Q.G., Rushton, A.W.A., 2008. New age constraints for the Ordovician Tyrone Volcanic Group, Northern Ireland. *J. Geol. Soc. Lond.* 165, 333–339.
- Cowan, C.A., Fox, D.L., Runkel, A.C., Saltzman, M.R., 2005. Terrestrial–marine carbon cycle coupling in similar to 500-m.y.-old phosphatic brachiopods. *Geology* 33, 661–664.
- Crowell, J.C., 1999. Pre-Mezozoic Ice Ages: Their Bearing on Understanding the Climate System. Memoir 192, Geological Society of America, 112 p.
- Davidek, K., Landing, E., Bowring, S.A., Westrop, S.R., Rushton, A.W.A., Fortey, R.A., Adrain, J.M., 1998. New uppermost Cambrian U–Pb date from Avalonian Wales and age of the Cambrian–Ordovician boundary. *Geol. Mag.* 135, 305–309.
- Emerson, N.R., Simo, J.A., Byers, C.W., Fournelle, J., 2004. Correlation of (Ordovician, Mohawkian) K-bentonites in the upper Mississippi valley using apatite chemistry: implications for stratigraphic interpretation of the mixed carbonate–siliclastic Decorah Formation. *Palaeogeogr. Palaeoclimatol. Palaeoecol.* 210, 215–233.
- Ethington, R.L., 1959. Conodonts of the Ordovician Galena Formation. *J. Paleontol.* 33, 257–292.
- Fan, J., Peng, P., Melchin, M.J., 2009. Carbon isotopes and event stratigraphy near the Ordovician–Silurian boundary, Yichang, South China. *Palaeogeogr. Palaeoclimatol. Palaeoecol.* 276, 160–169.
- Fanton, K.C., Holmden, C., 2007. Sea-level forcing of carbon isotope excursions in epeiric seas: implications for chemostratigraphy. *Can. J. Earth Sci.* 44, 807–818.
- Fortey, R.A., Harper, D.A.T., Ingham, J.K., Owen, A.W., Parkes, M.A., Rushton, A.W.A., Woodcock, N.H., 2000. A Revised Correlation of Ordovician Rocks in the British Isles. Special Report 24, The Geological Society, London, 83 p.
- Frakes, L.A., Francis, J.E., Syktus, J.I., 1992. *Climate Modes of the Phanerozoic*. Cambridge University Press, Cambridge, 274 p.
- Ghienne, J.-F., 2003. Late Ordovician sedimentary environments, glacial cycles, and post-glacial transgression in the Taoudeni Basin, West Africa. *Palaeogeogr. Palaeoclimatol. Palaeoecol.* 189, 117–145.
- Goldman, D., Bergström, S.M., 1997. Late Ordovician graptolites from the North American midcontinent. *Palaentology* 40, 965–1010.
- Haq, B., Hardenbol, J., Vail, P., 1987. Chronology of fluctuating sea levels since the Triassic. *Science* 235, 1156–1167.
- Hatch, J.R., Jacobson, S.R., Witzke, B.J., Risatti, J.B., Anders, D.E., Watney, W.L., Newell, K.D., Vuletic, A.K., 1987. Possible late Middle Ordovician organic carbon isotope excursion: evidence from Ordovician oils and hydrocarbon source rocks, mid-continent and east-central United States. *Am. Assoc. Pet. Geol. Bull.* 71, 1342–1354.
- Hay, R.L., Lee, M.C., Kolata, D.R., Matthews, J.C., Morton, J.P., 1988. Episodic potassic diagenesis of Ordovician tuffs in the Mississippi valley area. *Geology* 16, 743–747.
- Haynes, J.T., 1994. The Ordovician Deicke and Millbrig K-bentonite beds of the Cincinnati Arch and the southern valley and ridge province. Special Paper 290, Geological Society of America, 80 p.
- Huff, W.D., Bergström, S.M., Kolata, D.R., 1992. Gigantic Ordovician volcanic ash fall in North America and Europe: biological, tectonomagmatic, and event-stratigraphic significance. *Geology* 20, 875–878.
- Huff, W.D., Bergström, S.M., Kolata, D.L., 2010. Ordovician explosive volcanism. In: Finney, S.C., Berry, W.B.N. (Eds.), *The Ordovician Earth System*. Special Paper 466, Geological Society of America, pp. 13–28.
- Jacobson, S.R., Finney, S., Hatch, J.R., Ludvigson, G.A., 1995. *Gloeocapsomorpha prisca*-driven organic carbon isotope excursion, late Middle Ordovician (Rocklandian), North American mid-continent: new data from Nevada and Iowa. In: Cooper, J.D., Droser, M.L., Finney, S.C. (Eds.), *Ordovician Odyssey: Short Papers for the Seventh International Symposium on the Ordovician System*, Las Vegas, NV. Pacific Section SEPM (Society for Sedimentary Geology), pp. 305–308.
- Kaljo, D., Martma, T., Saadre, T., 2007. Post-Hunnebergian Ordovician carbon isotope trend in Baltoscandia, its environmental implications and some similarities with that of Nevada. *Palaeogeogr. Palaeoclimatol. Palaeoecol.* 245, 138–155.
- Kaufmann, B., 2006. Calibrating the Devonian time scale: a synthesis of U–Pb ID-TIMS ages and conodont stratigraphy. *Earth Sci. Rev.* 76, 175–190.
- Kolata, D.R., Huff, W.D., Bergström, S.M., 1996. Ordovician K-Bentonites of Eastern North America. Special Paper 313, Geological Society of America 84 p.
- Kolata, D.R., Huff, W.D., Bergström, S.M., 1998. Nature and regional significance of unconformities associated with the Middle Ordovician Hagan K-bentonite complex in the North American midcontinent. *Geol. Soc. Am. Bull.* 110, 723–739.
- Kolata, D.R., Huff, W.D., Bergström, S.M., 2001. The Ordovician Sebree Trough: an oceanic passage to the Midcontinent United States. *Geol. Soc. Am. Bull.* 113, 1067–1078.
- Kuiper, K.F., Deino, A., Hilgen, F.J., Krijgsman, W., Renne, P.R., Wijbrans, J.R., 2008. Synchronizing rock clocks of earth history. *Science* 320, 500–504.
- Kump, L.R., Arthur, M.A., Patzkowsky, M.E., Gibbs, M.T., Pinkus, D.S., Sheehan, P.M., 1999. A weathering hypothesis for glaciation at high atmospheric  $p\text{CO}_2$  during the Late Ordovician. *Palaeogeogr. Palaeoclimatol. Palaeoecol.* 152, 173–187.
- Landing, E., Bowring, S.A., Fortey, R.A., Davidek, K.L., 1997. U–Pb zircon date from Avalonian Cape Breton Island and geochronological calibration of the early Ordovician. *Can. J. Earth Sci.* 34, 724–730.
- Landing, E., Bowring, S.A., Davidek, K.L., Rushton, A.W.A., Fortey, R.A., Wimbledon, W.A.P., 2000. Cambrian–Ordovician boundary age and duration of the lowest Ordovician Tremadoc Series based on U–Pb zircon dates from Avalonian Wales. *Geol. Mag.* 137, 485–494.
- LaPorte, D.F., Holmden, C., Patterson, W.P., Loxton, J.D., Melchin, M.J., Mitchell, C.E., Finney, S.C., Sheets, H.D., 2009. Local and global perspectives on carbon and nitrogen cycling during the Hirnantian glaciation. *Palaeogeogr. Palaeoclimatol. Palaeoecol.* 276, 182–195.
- Leslie, S.A., 2000. Mohawkian (Upper Ordovician) conodonts of eastern North America and Baltoscandia. *J. Paleontol.* 74, 1122–1147.
- Leslie, S.A., Bergström, S.M., 2005. Conodont biostratigraphy across the Turinian–Chatfieldian stage transition (Late Ordovician, Mohawkian) in the upper

- Mississippi Valley. In: Ludvigson, G.A., Bunker, B.J. (Eds.), Facets of the Ordovician Geology of the Upper Mississippi Valley Region. Guidebook 24, Iowa Geological Survey, pp. 31–34.
- Lindström, M., 1971. Lower Ordovician conodonts of Europe. In: Sweet, W.C., Bergström, S.M. (Eds.), Symposium on Conodont Biostratigraphy, Memoir 127. Geological Society of America, p. 21–61.
- Ludvigson, G.A., Witzke, B.J., González, L.A., Carpenter, S.J., Schneider, C.L., Hasiuk, F., 2004. Late Ordovician (Turinian–Chatfieldian) carbon isotope excursions and their stratigraphic and paleoceanographic significance. *Palaeogeogr. Palaeoclimatol. Palaeoecol.* 210, 187–214.
- Marshall, J.D., Middleton, P.D., 1990. Changes in marine isotopic composition and the Late Ordovician glaciation. *J. Geol. Soc. Lond.* 147, 1–4.
- Mattinson, J.M., 2005. Zircon U/Pb chemical abrasion (CA-TIMS) method; combined annealing and multi-step partial dissolution analysis for improved precision and accuracy of zircon ages. *Chem. Geol.* 220, 47–66.
- Miller, K.G., Wright, J.D., Fairbanks, R.G., 1991. Unlocking the ice house; Oligocene–Miocene oxygen isotopes, eustasy, and margin erosion. *J. Geophys. Res.* 96, 6829–6848.
- Min, K., Renne, P.R., Huff, W.D., 2001.  $^{40}\text{Ar}/^{39}\text{Ar}$  dating of Ordovician K-bentonites in Laurentia and Baltoscandia. *Earth Planet. Sci. Lett.* 185, 121–134.
- Mitchell, C.E., Adhya, S., Bergström, S.M., Joy, M.P., Delano, J.W., 2004. Discovery of the Ordovician Millbrig K-bentonite Bed in the Trenton Group of New York State: implications for regional correlation and sequence stratigraphy in eastern North America. *Palaeogeogr. Palaeoclimatol. Palaeoecol.* 210, 331–346.
- Mossler, J.H., Hayes, J.B., 1966. Ordovician potassium bentonites of Iowa. *J. Sediment. Petrol.* 36, 414–427.
- Mussman, J.F., Read, J.F., 1986. Sedimentology and development of a passive margin unconformity: Middle Ordovician Knox unconformity, Virginia Appalachians. *Geol. Soc. Am. Bull.* 97, 282–295.
- Nielsen, A.T., 2004. Ordovician sea level changes: A Baltoscandian perspective. In: Webby, B.D., Paris, F., Droser, M.L., Percival, I.G. (Eds.), The Great Ordovician Biodiversification Event. Columbia University Press, New York, pp. 84–93.
- Patzkowsky, M.E., Holland, S.M., 1997. Patterns of turnover in Middle and Upper Ordovician brachiopods of the eastern United States: a test of coordinated stasis. *Paleobiology* 23, 420–443.
- Patzkowsky, M.E., Slupik, L.M., Arthur, M.A., Pancost, R.D., Freeman, K.H., 1997. Late Middle Ordovician environmental change and extinction: harbinger of the Late Ordovician or continuation of Cambrian patterns? *Geology* 25, 911–914.
- Paul, H.A., Zachos, J., Flower, B.P., Tripartit, A., 2000. Orbitally induced climate and geochemical variability across the Oligocene/Miocene boundary. *Paleoceanography* 15, 471–485.
- Pope, M.C., Steffen, J.B., 2003. Widespread, prolonged late Middle to Late Ordovician upwelling in North America: a proxy record of glaciation? *Geology* 31, 63–66.
- Prokoph, A., Shields, G.A., Veizer, J., 2008. Compilation and time-series analysis of a marine carbonate  $\delta^{18}\text{O}$ ,  $\delta^{13}\text{C}$ ,  $^{87}\text{Sr}/^{86}\text{Sr}$  and  $\delta^{34}\text{S}$  database through Earth history. *Earth Sci. Rev.* 87, 113–133.
- Qing, H., Barnes, C.R., Buhl, D., Veizer, J., 1998. The strontium isotopic composition of Ordovician and Silurian brachiopods and conodonts: relationship to geological events and implications for coeval seawater. *Geochim. Cosmochim. Acta* 62, 1721–1733.
- Raymo, M.E., Ruddiman, W.F., Froehlich, P.N., 1988. Influence of late Cenozoic mountain building on ocean geochemical cycles. *Geology* 16, 649–653.
- Renne, P.R., Swisher, C.C., Deino, A.L., Karner, D.B., Owens, T.L., DePaolo, D.J., 1998. Intercalibration of standards, absolute ages and uncertainties in  $^{40}\text{Ar}/^{39}\text{Ar}$  dating. *Chem. Geol.* 145, 117–152.
- Renne, P.R., Mundil, R., Balco, G., Min, K., Ludwig, K.R., 2010. Joint determination of  $^{40}\text{K}$  decay constants and  $^{40}\text{Ar}/^{40}\text{K}$  for the Fish Canyon sanidine standard, and improved accuracy for  $^{40}\text{Ar}/^{39}\text{Ar}$  geochronology. *Geochim. Cosmochim. Acta* 74, 5349–5367.
- Richardson, J.G., Bergström, S.M., 2003. Regional stratigraphic relations of the Trenton Limestone (Chatfieldian) in the eastern North American midcontinent. *Northeast. Geol. Environ. Sci.* 18, 93–115.
- Rowan, E.L., Goldhaber, M.B., 1995. Duration of mineralization and fluid-flow history of the upper Mississippi Valley zinc–lead district. *Geology* 23, 609–612.
- Sadler, P.M., Cooper, R.A., 2004. Calibration of the Ordovician timescale. In: Webby, B.D., Paris, F., Droser, M.L., Percival, I.G. (Eds.), The Great Ordovician Biodiversification Event. Columbia University Press, New York, pp. 48–51.
- Sadler, P.M., Cooper, R.A., Melchin, M., 2009. High-resolution, early Paleozoic (Ordovician–Silurian) time scales. *Geol. Soc. Am. Bull.* 121, 887–906.
- Salamy, K.A., Zachos, J., 1999. Latest Eocene–early Oligocene climate change and Southern Ocean fertility; inferences from sediment accumulation and stable isotope data. *Palaeogeogr. Palaeoclimatol. Palaeoecol.* 145, 61–77.
- Saltzman, M.R., 2005. Phosphorus, nitrogen, and the redox evolution of the Paleozoic oceans. *Geology* 33, 573–576.
- Saltzman, M.R., Young, S.A., 2005. Long-lived glaciation in the Late Ordovician? Isotopic and sequence-stratigraphic evidence from western Laurentia. *Geology* 33, 109–112.
- Saltzman, M.M., Bergström, S.M., Huff, W.D., Kolata, D.R., 2003. Conodont and graptolite biostratigraphy and the Ordovician (Early Chatfieldian, Middle Caradocian)  $\delta^{13}\text{C}$  excursion in North America and Baltoscandia: implications for the interpretation of the relations between the Millbrig and Kinnekulle K-bentonites. In: Albanesi, G.L., Beresi, M.S., Peralta, S.H. (Eds.), 9th International Symposium on the Ordovician System: Ordovician from the Andes. Volume 17, Instituto Superior de Correlación Geológica (INSUGEO), pp. 137–142.
- Saltzman, M.R., Cowan, C.A., Runkel, A.C., Runnegar, B., Stewart, M.C., Palmer, A.R., 2004. The Late Cambrian SPICE ( $\delta^{13}\text{C}$ ) event and the Sauk II–Sauk III regression: new evidence from Laurentian basins in Utah, Iowa, and Newfoundland. *J. Sediment. Res.* 74, 366–377.
- Schmitz, B., Bergström, S.M., 2007. Chemostratigraphy in the Swedish Upper Ordovician: regional significance of the Hirnantian  $\delta^{13}\text{C}$  excursion (HICE) in the Boda Limestone of the Siljan region. *GFF* 129, 133–140.
- Schmitz, B., Bergström, S.M., Wang, X.F., 2010. The middle Darriwilian (Ordovician)  $\delta^{13}\text{C}$  excursion (MDICE) discovered in the Yangtze Platform succession in China: implications of its first recorded occurrences outside Baltoscandia. *J. Geol. Soc. Lond.* 167, 249–259.
- Schoene, B., Crowley, J.L., Condon, D.J., Schmitz, M.D., Bowring, S.A., 2006. Reassessing the uranium decay constants for geochronology using ID-TIMS U–Pb data. *Geochim. Cosmochim. Acta* 70, 426–445.
- Sepkoski Jr., J.J., 1995. The Ordovician radiations: diversification and extinction shown by global genus-level taxonomic data. In: Cooper, J.D., Droser, M.L., Finney, S.C. (Eds.), Ordovician Odyssey: Short Papers for the Seventh International Symposium on the Ordovician System, Las Vegas, NV, Pacific Section SEPM (Society for Sedimentary Geology), pp. 393–396.
- Shields, G.A., Carden, G.A.F., Veizer, J., Meidla, T., Rong, J.Y., Li, R.Y., 2003. Sr, C and O isotope geochemistry of Ordovician brachiopods: a major isotopic event around the Middle–Late Ordovician transition. *Geochim. Cosmochim. Acta* 67, 2005–2025.
- Simo, J.A., Emerson, N.R., Byers, C.W., Ludvigson, G.A., 2003. Anatomy of an embayment in an Ordovician epeiric sea, Upper Mississippi Valley, USA. *Geology* 31, 545–548.
- Sloss, L.L., 1963. Sequences in the cratonic interior of North America. *Geol. Soc. Am. Bull.* 74, 93–114.
- Smith, M.E., Singer, B.S., Carroll, A.R., Fournelle, J.H., 2008. Precise dating of biotite in distal ash: isolating subtle alteration using  $^{40}\text{Ar}/^{39}\text{Ar}$  laser incremental heating and electron microprobe techniques. *Am. Mineral.* 93, 784–795.
- Smith, M.E., Chamberlain, K.R., Singer, B.S., Carroll, A.R., 2010. Eocene clocks agree: coeval  $^{40}\text{Ar}/^{39}\text{Ar}$ , U–Pb, and astronomical ages from the Green River Formation. *Geology* 38, 527–530.
- Steiger, R.H., Jäger, E., 1977. Subcommittee on geochronology: convention on the use of decay constants in geo- and cosmochronology. *Earth Planet. Sci. Lett.* 36, 359–362.
- Sweet, W.C., 1979a. Conodonts and conodont biostratigraphy of post-Tyrone Ordovician rocks of the Cincinnati region. Professional Paper 1066-G. United States Geological Survey, pp. 1–26.
- Sweet, W.C., 1979b. Late Ordovician conodonts and biostratigraphy of the western midcontinent province. Brigham Young Univ. Geol. Stud. 26, 45–85.
- Sweet, W.C., 1984. Graphic correlation of Middle and Upper Ordovician rocks, North American midcontinent province, U.S.A. In: Bruton, D.L. (Ed.), Aspects of the Ordovician System. Paleontological Contributions from the University of Oslo. Volume 295, pp. 23–35.
- Sweet, W.C., 1987. Distribution and significance of conodonts in Middle and Upper Ordovician strata of the upper Mississippi valley region. In: Sloan, R.E. (Ed.), Middle and Late Ordovician Lithostratigraphy and Biostratigraphy of the Upper Mississippi Valley. Report of Investigations 35, Minnesota Geological Survey, pp. 167–172.
- Sweet, W.C., 1995. A conodont-based composite standard for the North American Ordovician. In: Cooper, J.D., Droser, M.L., Finney, S.C. (Eds.), Ordovician Odyssey: Short Papers for the Seventh International Symposium on the Ordovician System, Las Vegas, NV. Pacific Section SEPM (Society for Sedimentary Geology), pp. 15–20.
- Sweet, W.C., 2005. Graphical refinement of the conodont database: examples and a plea. In: Purnell, M.A., Donoghue, P.C.J. (Eds.), Conodont Biology and Phylogeny: Interpreting the Fossil Record. Special Papers in Paleontology Series, 73, pp. 135–141.
- Sweet, W.C., Bergström, S.M., 1971. The American Upper Ordovician standard: XIII. A revised time-stratigraphic classification of North American upper Middle and Upper Ordovician rocks. *Geol. Soc. Am. Bull.* 82, 613–628.
- Sweet, W.C., Tolbert, C.M., 1997. An Ibeixian (Lower Ordovician) reference section in the southern Egan Range, Nevada, for a conodont-based chronostratigraphy. Professional Paper 1579-B. United States Geological Survey, pp. 51–84.
- Sweet, W.C., Ethington, R.L., Harris, A.G., 2005. A conodont-based standard reference section in central Nevada for the lower Middle Ordovician Whiterockian Series. *Bull. Am. Paleontol.* 369, 35–52.
- Templeton, J.S., Willman, H.B., 1963. Champlainian Series (Middle Ordovician) in Illinois Bulletin 89, Illinois State Geological Survey, p. 91.
- Thompson Jr., W.H., 1959. Conodonts of the Platteville Formation of Southeastern Minnesota. M.S. Thesis, University of Minnesota, Minneapolis, 168 p.
- Tucker, R.D., 1991. Ordovician and Silurian Stratotypes of Britain. Open-File Report 91–565. United States Geological Survey, pp. 57–58.
- Tucker, R.D., McEerrow, W.S., 1995. Early Paleozoic chronology: a review in light of new U–Pb zircon ages from Newfoundland and Britain. *Can. J. Earth Sci.* 32, 368–379.
- Tucker, R.D., Krogh, T.E., Ross, R.J., Williams, S.H., 1990. Time-scale calibration by high-precision U–Pb zircon dating of interstratified volcanic ashes in the Ordovician and Lower Silurian stratotypes of Britain. *Earth Planet. Sci. Lett.* 100, 51–58.
- Votaw, R.B., 1971. Conodont biostratigraphy of the Black River Group (Middle Ordovician) and equivalent rocks of the eastern midcontinent, North America. North America. Ph.D. Thesis, The Ohio State University, Columbus, 170 p.
- Webby, B.D., Van den Berg, A.H.M., Cooper, R.A., Stewart, I., Shergold, J.H., Nicoll, R.S., Burrett, C.F., Stait, B., Cooper, B.J., Laurie, J., Sherwin, L., 1991. Subdivisions of the Ordovician System in Australia. In: Barnes, C.R., Williams, S.H. (Eds.), Advances in Ordovician Geology. Paper 90–9, Geological Survey of Canada, pp. 47–57.
- Webby, B.D., Cooper, R.A., Bergström, S.M., Paris, F., 2004. Stratigraphic framework and time slices. In: Webby, B.D., Paris, F., Droser, M.L., Percival, I.G. (Eds.), The Great Ordovician Biodiversification Event. Columbia University Press, New York, pp. 41–47.

- Webers, G.F., 1966. The Middle and Upper Ordovician conodont faunas of Minnesota, Special Publication SP-4, Minnesota Geological Survey, 123 p.
- Wendt, I., Carl, C., 1991. The statistical distribution of the mean squared weighted deviation. *Chem. Geol.* 86, 275–285.
- Willman, H.B., Kolata, D.R., 1978. The Platteville and Galena Groups in Northern Illinois, Circular 502. Illinois State Geological Survey, 75 p.
- Witzke, B.J., Ludvigson, G.A., 2005. The Ordovician Galena Group in Iowa and its regional stratigraphic relationships. In: Ludvigson, G.A., Bunker, B.J. (Eds.), *Facets of the Ordovician Geology of the Upper Mississippi Valley Region*. Guidebook 24. Iowa Geological Survey, pp. 3–22.
- Young, S.A., Saltzman, M.R., Foland, K.A., Linder, J.S., Kump, L.R., 2009. A major drop in seawater  $^{87}\text{Sr}/^{86}\text{Sr}$  during the Middle Ordovician (Darriwilian): links to volcanism and climate? *Geology* 37, 951–954.
- Young, S.A., Saltzman, M.R., Ausich, W.I., Desrochers, A., Kaljo, D., 2010. Did changes in atmospheric  $\text{CO}_2$  coincide with latest Ordovician glacial–interglacial cycles? *Palaeogeogr. Palaeoclimatol. Palaeoecol.* 296, 376–388.
- Zachos, J., Pagani, M., Sloan, L., Thomas, E., Billups, K., 2001. Trends, rhythms, and aberrations in global climate 65 Ma to present. *Science* 292, 685–693.



**Supplementary Figure 1.** Plots showing apparent  $^{40}\text{Ar}/^{39}\text{Ar}$  ages from sanidine fusions versus the percentage of radiogenic  $^{40}\text{Ar}^*$  illustrating correlation between skew towards younger ages and less radiogenic grains. Dashed vertical line represents the  $>96\%$   $^{40}\text{Ar}^*$  limit used to filter data (see Supplementary Information Table S1 for details). Grey shaded ages are included in weighted mean age calculations. Shaded bar represents Rb-Sr age for sphalerite formed during Mississippi Valley type (MVT) mineralization in the UMV (Brannon et al. 1992).

SUPPLEMENTARY TABLE 1. LASER FUSION  $^{40}\text{Ar}/^{39}\text{Ar}$  RESULTS

Sample Experiment	$^{40}\text{Ar}/^{39}\text{Ar}$	$^{37}\text{Ar}/^{39}\text{Ar}$	$^{36}\text{Ar}/^{39}\text{Ar}$	$^{40}\text{Ar}^*$ X10 <sup>-14</sup> mol	$^{40}\text{Ar}^*$ %	K/Ca	Apparent Age ± 2σ Ma
<b>Millbrig bentonite sanidine</b> $J = 0.010631 \pm 0.15\%$ $\mu = 1.0050$							
BB6211	26.980 ± 0.056	0.00559 ± 0.00048	0.000813 ± 0.000245	3.24	99.1	76.9	451.36 ± 2.73
BB6213	27.075 ± 0.127	0.00475 ± 0.00122	0.001130 ± 0.000518	1.42	98.8	90.4	451.38 ± 5.91
BB6214	26.797 ± 0.078	0.00676 ± 0.00060	0.000804 ± 0.000268	2.53	99.1	63.7	448.67 ± 3.31
BB6217	27.108 ± 0.059	0.00545 ± 0.00077	0.000757 ± 0.000289	2.24	99.2	78.9	453.51 ± 3.09
BB6220	26.781 ± 0.101	0.00504 ± 0.00106	0.000979 ± 0.000538	1.34	98.9	85.4	447.65 ± 5.62
BB6222	26.970 ± 0.071	0.00523 ± 0.00038	0.000848 ± 0.000233	3.03	99.1	82.2	451.06 ± 2.94
BB6223	26.909 ± 0.144	0.00477 ± 0.00095	0.001214 ± 0.000577	1.29	98.7	90.1	448.53 ± 6.64
BB6225	27.349 ± 0.105	0.00308 ± 0.00140	0.001367 ± 0.000726	0.91	98.5	139.5	454.42 ± 7.11
BB6226	27.063 ± 0.066	0.00448 ± 0.00061	0.001025 ± 0.000440	1.98	98.9	96.0	451.67 ± 4.35
BB6228	26.913 ± 0.065	0.00497 ± 0.00033	0.000581 ± 0.000144	5.74	99.4	86.6	451.39 ± 2.32
BB6229	26.899 ± 0.088	0.00536 ± 0.00047	0.000617 ± 0.000211	4.34	99.3	80.2	451.02 ± 3.21
BB6232	26.891 ± 0.056	0.00497 ± 0.00061	0.000740 ± 0.000246	2.76	99.2	86.6	450.35 ± 2.74
BB6234	27.058 ± 0.106	0.00716 ± 0.00107	0.001242 ± 0.000476	1.43	98.6	60.0	450.63 ± 5.24
BB6235	26.973 ± 0.084	0.00473 ± 0.00090	0.001011 ± 0.000376	1.45	98.9	90.9	450.39 ± 4.15
** BB6237	25.316 ± 0.035	0.00947 ± 0.00024	0.000796 ± 0.000140	6.75	99.1	45.4	426.42 ± 1.63
BB6240	27.134 ± 0.101	0.00487 ± 0.00054	0.000787 ± 0.000283	2.64	99.1	88.3	453.77 ± 3.90
* BB6241	28.113 ± 0.083	0.00544 ± 0.00040	0.004156 ± 0.000279	3.32	95.6	79.0	453.52 ± 3.42
** BB6243	26.141 ± 0.091	0.00535 ± 0.00082	0.000941 ± 0.000468	1.61	98.9	80.4	438.22 ± 4.97
BB6244	27.104 ± 0.073	0.00438 ± 0.00083	0.000819 ± 0.000499	1.65	99.1	98.2	453.19 ± 4.91
BB6247	27.350 ± 0.157	0.00324 ± 0.00161	0.001552 ± 0.000868	0.84	98.3	132.6	453.63 ± 8.93
BB6249	27.272 ± 0.065	0.00545 ± 0.00053	0.000983 ± 0.000254	2.92	98.9	78.9	454.96 ± 2.96
BB6250	27.181 ± 0.084	0.00682 ± 0.00076	0.001191 ± 0.000428	1.97	98.7	63.0	452.69 ± 4.51
BB6252	27.408 ± 0.136	0.00507 ± 0.00144	0.001448 ± 0.000849	0.90	98.4	84.9	454.95 ± 8.48
** BB7006	25.666 ± 0.095	0.00692 ± 0.00092	0.000588 ± 0.000325	2.24	99.3	62.1	432.63 ± 4.07
BB7007	27.244 ± 0.097	0.00498 ± 0.00159	0.001176 ± 0.000563	1.18	98.7	86.4	453.69 ± 5.73
BB7009	26.930 ± 0.058	0.00562 ± 0.00084	0.000615 ± 0.000308	4.01	99.3	76.4	451.48 ± 3.21
BB7010	27.015 ± 0.099	0.00538 ± 0.00123	0.000951 ± 0.000362	1.54	99.0	79.9	451.27 ± 4.35
BB7012	26.828 ± 0.072	0.00417 ± 0.00092	0.000655 ± 0.000301	2.19	99.3	103.1	449.78 ± 3.42
BB7013	27.133 ± 0.063	0.00572 ± 0.00167	0.000793 ± 0.000380	1.60	99.1	75.2	453.73 ± 3.83
BB7015	26.865 ± 0.101	0.00513 ± 0.00060	0.000552 ± 0.000266	3.96	99.4	83.8	450.78 ± 3.81
BB7016	26.861 ± 0.129	0.00526 ± 0.00161	0.001047 ± 0.000675	1.10	98.8	81.7	448.55 ± 7.08
BB7018	27.034 ± 0.044	0.00403 ± 0.00073	0.000716 ± 0.000295	3.01	99.2	106.7	452.59 ± 2.91
BB7021	26.946 ± 0.105	0.00479 ± 0.00124	0.001109 ± 0.000454	1.42	98.8	89.7	449.55 ± 5.08
BB7022	26.879 ± 0.065	0.00539 ± 0.00103	0.000945 ± 0.000348	2.19	99.0	79.7	449.27 ± 3.62
BB7024	27.143 ± 0.091	0.00539 ± 0.00094	0.000827 ± 0.000386	2.32	99.1	79.8	453.73 ± 4.34
BB7038	26.804 ± 0.089	0.00475 ± 0.00123	0.001013 ± 0.000373	1.89	98.9	90.5	447.85 ± 4.23
BB7040	26.887 ± 0.088	0.00524 ± 0.00082	0.000834 ± 0.000199	2.19	99.1	82.1	449.88 ± 3.15
BB7041	27.271 ± 0.177	0.00607 ± 0.00256	0.001875 ± 0.000728	0.74	98.0	70.8	451.02 ± 8.26
BB7043	26.907 ± 0.115	0.00598 ± 0.00174	0.001012 ± 0.000481	1.27	98.9	71.9	449.40 ± 5.44
BB7044	27.781 ± 0.081	0.00703 ± 0.00081	0.002276 ± 0.000250	2.68	97.6	61.2	456.86 ± 3.22
BB7046	26.905 ± 0.090	0.00517 ± 0.00075	0.000699 ± 0.000301	2.49	99.2	83.1	450.73 ± 3.77
BB7047	27.216 ± 0.086	0.00631 ± 0.00134	0.000820 ± 0.000307	1.74	99.1	68.1	454.86 ± 3.71
BB7050	27.877 ± 0.118	0.00541 ± 0.00128	0.000662 ± 0.000424	1.38	99.3	79.5	465.36 ± 5.08
BB7053	26.955 ± 0.066	0.00425 ± 0.00052	0.000571 ± 0.000215	3.42	99.4	101.2	452.05 ± 2.73
BB7695	26.805 ± 0.207	0.00437 ± 0.00310	0.000783 ± 0.000682	0.92	99.1	98.4	448.88 ± 8.61
BB7696	26.403 ± 0.145	0.00028 ± 0.00280	0.000788 ± 0.000665	0.94	99.1	151.1	442.82 ± 7.32
BB7698	27.164 ± 0.111	0.00625 ± 0.00247	0.000804 ± 0.000626	1.14	99.1	68.8	454.15 ± 6.42
BB7699	26.841 ± 0.057	0.00416 ± 0.00162	0.000962 ± 0.000288	2.08	98.9	103.4	448.61 ± 3.07
** BB7701	25.130 ± 0.105	0.02693 ± 0.00336	0.002166 ± 0.000973	0.76	97.5	16.0	417.48 ± 9.30
BB7702	27.091 ± 0.093	0.00374 ± 0.00178	0.000746 ± 0.000374	1.66	99.2	114.9	453.30 ± 4.30
BB7704	27.075 ± 0.142	0.00842 ± 0.00256	0.001128 ± 0.000514	1.14	98.8	51.1	451.39 ± 6.19
BB7705	26.988 ± 0.082	0.00386 ± 0.00128	0.001284 ± 0.000399	2.12	98.6	111.5	449.40 ± 4.29
BB7707	26.895 ± 0.079	0.00441 ± 0.00093	0.000614 ± 0.000228	2.85	99.3	97.5	450.97 ± 3.10
BB7708	27.010 ± 0.083	0.00693 ± 0.00112	0.000757 ± 0.000353	2.67	99.2	62.0	452.05 ± 3.98
BB7710	27.120 ± 0.085	0.00612 ± 0.00175	0.000939 ± 0.000315	2.33	99.0	70.2	452.89 ± 3.75
* BB7711	28.584 ± 0.363	0.00529 ± 0.00943	0.004517 ± 0.002108	0.33	95.3	81.2	458.95 ± 21.29
BB7713	27.034 ± 0.118	0.00469 ± 0.00203	0.001150 ± 0.000380	1.50	98.7	91.7	450.67 ± 4.85
Inverse isochron age ± 2σ	443.80 ± 3.75					Integrated age ± 2σ	449.45 ± 1.31
$^{40}\text{Ar}/^{39}\text{Ar}$ intercept ± 2σ	908.3 ± 365.7		MSWD 1.73			Weighted mean age ± 2σ	<b>451.67 ± 1.40</b>

SUPPLEMENTARY TABLE 1. LASER FUSION <sup>40</sup>Ar/<sup>39</sup>Ar RESULTS

Sample Experiment	<sup>40</sup> Ar/ <sup>39</sup> Ar	<sup>37</sup> Ar/ <sup>39</sup> Ar	<sup>36</sup> Ar/ <sup>39</sup> Ar	<sup>40</sup> Ar* X10 <sup>-14</sup> mol	<sup>40</sup> Ar* %	K/Ca	Apparent Age ± 2σ Ma
<b>Dygerts bentonite sanidine</b> $J = 0.014694 \pm 0.14\%$ $\mu = 1.0025$							
BA5364	19.292 ± 0.031	0.01462 ± 0.00022	0.000139 ± 0.000066	10.66	99.8	29.4	449.38 ± 1.53
BA5380	19.270 ± 0.023	0.04253 ± 0.00041	0.000239 ± 0.000098	9.48	99.6	10.1	448.35 ± 1.52
BA5381	19.375 ± 0.034	0.03847 ± 0.00080	0.000493 ± 0.000306	2.03	99.2	11.2	448.98 ± 3.99
* BA5384	32.466 ± 1.863	2.26544 ± 0.12974	0.030884 ± 0.026275	0.03	72.4	0.2	536.21 ± 310.8
* BA5749	18.292 ± 10.041	0.39105 ± 0.01827	0.041095 ± 0.031589	0.09	33.8	1.1	156.77 ± 666.1
* BA5751	28.837 ± 25.508	0.60220 ± 0.04020	0.056803 ± 0.080717	0.05	41.9	0.7	295.27 ± 1572
BA5752	19.428 ± 0.199	0.01387 ± 0.00037	0.000647 ± 0.000623	4.77	99.0	31.0	449.07 ± 11.20
BA5754	18.976 ± 0.240	0.01950 ± 0.00061	0.000698 ± 0.000741	3.88	98.9	22.1	439.42 ± 13.51
* BA5755	17.555 ± 2.171	0.06244 ± 0.00355	0.015320 ± 0.006992	0.39	74.2	6.9	316.07 ± 133.4
* BA5757	21.108 ± 0.153	0.14389 ± 0.00130	0.006427 ± 0.000484	6.82	91.0	3.0	448.76 ± 8.65
* BA5763	21.788 ± 1.540	0.38238 ± 0.00498	0.017231 ± 0.004811	0.68	76.8	1.1	396.50 ± 89.20
BA5764	18.973 ± 0.486	1.02307 ± 0.00840	0.002441 ± 0.001578	1.90	96.6	0.4	430.55 ± 28.13
BA5766	19.498 ± 0.171	0.14597 ± 0.00135	0.001465 ± 0.000526	5.61	97.8	2.9	445.79 ± 9.57
BA5767	19.363 ± 0.220	0.04391 ± 0.00067	0.001662 ± 0.000684	4.31	97.5	9.8	441.59 ± 12.39
BA5770	19.355 ± 0.213	0.17194 ± 0.00188	0.002080 ± 0.000685	4.43	96.9	2.5	439.09 ± 12.20
* BA5772	18.984 ± 0.322	0.11256 ± 0.00106	0.003185 ± 0.001025	2.89	95.1	3.8	424.41 ± 18.53
* BA5773	30.468 ± 16.334	1.22100 ± 0.04639	0.046663 ± 0.052593	0.09	55.1	0.4	397.76 ± 959.2
* BA5775	20.856 ± 0.717	0.10438 ± 0.00164	0.008032 ± 0.002265	1.41	88.6	4.1	433.60 ± 40.88
BA5776	19.108 ± 0.320	0.01382 ± 0.00059	0.000007 ± 0.000995	2.91	100.0	31.1	446.36 ± 17.99
BA5778	19.163 ± 0.114	0.01216 ± 0.00022	0.000044 ± 0.000350	8.43	99.9	35.4	447.28 ± 6.37
BA5779	19.156 ± 0.235	0.01707 ± 0.00049	0.000007 ± 0.000749	3.99	100.0	25.2	447.37 ± 13.36
* BA5784	20.037 ± 0.487	0.20722 ± 0.00193	0.008810 ± 0.001624	2.00	87.1	2.1	411.80 ± 28.83
BA5796	19.382 ± 0.214	0.17150 ± 0.00167	0.000558 ± 0.000650	4.54	99.2	2.5	448.98 ± 11.89
* BA5899	20.020 ± 0.118	0.07973 ± 0.00107	0.003239 ± 0.000346	2.06	95.2	5.4	445.60 ± 6.45
* BA5900	20.025 ± 0.207	1.12388 ± 0.01168	0.004368 ± 0.000654	1.22	94.0	0.4	440.80 ± 11.72
** BA5902	5.101 ± 0.222	0.13122 ± 0.00325	0.000001 ± 0.000739	0.27	99.9	3.3	130.34 ± 10.95
* BA5903	22.611 ± 5.037	1.77299 ± 0.06822	0.037999 ± 0.014431	0.05	50.9	0.2	282.46 ± 298.0
BA5906	19.302 ± 0.070	0.06849 ± 0.00065	0.000283 ± 0.000186	4.05	99.6	6.3	448.80 ± 3.67
BA5920	19.198 ± 0.119	0.45522 ± 0.00425	0.000852 ± 0.000410	1.95	98.9	0.9	443.91 ± 7.02
BA5921	19.269 ± 0.082	0.09771 ± 0.00143	0.001011 ± 0.000270	3.05	98.5	4.4	443.72 ± 4.74
BA5924	19.388 ± 0.090	0.08208 ± 0.00143	0.000442 ± 0.000307	2.85	99.3	5.2	449.63 ± 5.29
* BA5926	9.788 ± 63.112	0.58876 ± 0.50291	0.005130 ± 0.196045	0.002	85.0	0.7	208.06 ± 4049
* BA6316	20.085 ± 0.061	0.03897 ± 0.00095	0.002966 ± 0.000235	3.28	95.6	11.0	448.54 ± 3.79
* BA6323	19.704 ± 0.230	0.07174 ± 0.00403	0.004126 ± 0.001367	0.59	93.8	6.0	433.58 ± 19.35
BA6325	19.574 ± 0.110	0.50369 ± 0.00637	0.002349 ± 0.000570	1.31	96.6	0.9	442.63 ± 8.33
* BA6326	20.367 ± 0.132	0.06532 ± 0.00140	0.005267 ± 0.000549	1.47	92.4	6.6	440.36 ± 8.58
* BA6328	19.848 ± 0.050	0.04131 ± 0.00117	0.003165 ± 0.000246	3.18	95.3	10.4	442.43 ± 3.64
* BA6329	19.970 ± 0.100	0.06137 ± 0.00152	0.003775 ± 0.000359	1.85	94.4	7.0	441.25 ± 5.98
BA6334	19.350 ± 0.066	0.01422 ± 0.00106	0.000468 ± 0.000325	2.51	99.3	30.2	448.58 ± 4.80
* BA6335	20.238 ± 0.148	0.05482 ± 0.00191	0.005495 ± 0.000567	1.29	92.0	7.8	436.25 ± 9.17
** BA6337	18.292 ± 0.079	0.01518 ± 0.00141	0.000256 ± 0.000412	1.60	99.6	28.3	427.86 ± 6.06
BA6338	19.982 ± 0.152	0.01847 ± 0.00160	0.002552 ± 0.000572	1.10	96.2	23.3	448.90 ± 9.33
BA6340	19.878 ± 0.081	0.02072 ± 0.00128	0.002098 ± 0.000313	2.19	96.9	20.8	449.53 ± 5.05
BA6344	19.566 ± 0.085	0.01797 ± 0.00110	0.000790 ± 0.000337	1.90	98.8	23.9	451.07 ± 5.39
* BA6349	20.857 ± 0.195	0.23509 ± 0.00438	0.015536 ± 0.000969	0.74	78.1	1.8	387.04 ± 14.70
** BA6352	18.748 ± 0.443	0.04327 ± 0.00533	0.001892 ± 0.002272	0.28	97.0	9.9	427.36 ± 33.64
* BA6358	24.686 ± 7.375	1.47872 ± 0.13758	0.016390 ± 0.033765	0.02	80.8	0.3	464.37 ± 507.7
BA6359	19.679 ± 0.046	0.12780 ± 0.00147	0.001653 ± 0.000140	4.18	97.6	3.4	448.34 ± 2.53
BA6361	19.249 ± 0.062	0.01126 ± 0.00057	0.000287 ± 0.000245	2.58	99.6	38.2	447.58 ± 3.96
BA6367	19.258 ± 0.091	0.01184 ± 0.00102	0.000353 ± 0.000284	2.07	99.4	36.3	447.36 ± 5.13
BA6368	19.446 ± 0.065	0.02050 ± 0.00087	0.001188 ± 0.000329	2.53	98.2	21.0	446.15 ± 4.83
** BA6371	18.437 ± 0.314	0.09839 ± 0.00351	0.000998 ± 0.001325	0.42	98.4	4.4	426.48 ± 20.97
* BA6373	24.541 ± 2.924	2.40299 ± 0.10425	0.011334 ± 0.016038	0.05	87.1	0.2	493.58 ± 224.5
# BA6374	23.916 ± 0.084	0.04343 ± 0.00130	0.002813 ± 0.000521	2.45	96.5	9.9	526.96 ± 6.93
* BA6379	23.868 ± 0.186	0.19809 ± 0.00340	0.022359 ± 0.000718	1.18	72.4	2.2	408.13 ± 11.17
BA6380	19.170 ± 0.052	0.01360 ± 0.00073	0.000376 ± 0.000227	3.00	99.4	31.6	445.40 ± 3.51
BA6382	19.613 ± 0.124	0.03389 ± 0.00188	0.001637 ± 0.000680	1.21	97.5	12.7	446.90 ± 9.76
** BA6391	18.024 ± 0.992	0.02911 ± 0.01880	0.000181 ± 0.004333	0.12	99.7	14.8	422.74 ± 67.93
BA6392	19.205 ± 0.075	0.01338 ± 0.00105	0.000306 ± 0.000355	1.96	99.5	32.1	446.55 ± 5.33
* BA6395	18.160 ± 0.146	0.07402 ± 0.00182	0.002711 ± 0.000479	1.07	95.6	5.8	409.95 ± 8.53
BA6398	20.198 ± 0.051	0.02663 ± 0.00061	0.002591 ± 0.000325	3.30	96.2	16.1	453.15 ± 4.47
BA6403	19.080 ± 0.214	0.01594 ± 0.00412	0.000013 ± 0.001230	0.64	100.0	27.0	445.76 ± 17.46

**SUPPLEMENTARY TABLE 1. LASER FUSION  $^{40}\text{Ar}/^{39}\text{Ar}$  RESULTS**

Sample Experiment	$^{40}\text{Ar}/^{39}\text{Ar}$	$^{37}\text{Ar}/^{39}\text{Ar}$	$^{36}\text{Ar}/^{39}\text{Ar}$	$^{40}\text{Ar}^*$ $\times 10^{-14}$ mol	$^{40}\text{Ar}^*$ %	K/Ca	Apparent Age $\pm 2\sigma$ Ma
<b>Dygerts bentonite cont...</b>							
** BA6407	18.103 $\pm$ 0.116	0.02708 $\pm$ 0.00130	0.001882 $\pm$ 0.000517	1.14	96.9	15.9	413.84 $\pm$ 8.06
BA6409	19.101 $\pm$ 0.087	0.01984 $\pm$ 0.00127	0.001227 $\pm$ 0.000337	1.73	98.1	21.7	438.76 $\pm$ 5.50
BA6412	19.288 $\pm$ 0.090	0.00976 $\pm$ 0.00106	0.000298 $\pm$ 0.000386	1.84	99.5	44.1	448.32 $\pm$ 6.01
BA6415	19.181 $\pm$ 0.106	0.01361 $\pm$ 0.00124	0.000107 $\pm$ 0.000468	1.46	99.8	31.6	447.28 $\pm$ 7.22
BA6418	19.464 $\pm$ 0.199	0.21283 $\pm$ 0.00444	0.002598 $\pm$ 0.001137	0.72	96.1	2.0	438.26 $\pm$ 16.21
* BA6424	18.839 $\pm$ 0.317	0.09553 $\pm$ 0.00564	0.005526 $\pm$ 0.001628	0.41	91.4	4.5	406.76 $\pm$ 24.27
BA6437	19.339 $\pm$ 0.125	0.01439 $\pm$ 0.00132	0.000008 $\pm$ 0.000510	1.20	100.0	29.9	451.15 $\pm$ 8.10
** BA6439	17.323 $\pm$ 0.143	0.00208 $\pm$ 0.00164	0.000082 $\pm$ 0.000825	0.88	99.8	207.0	408.56 $\pm$ 11.95
** BA6448	18.207 $\pm$ 0.075	0.00344 $\pm$ 0.00070	0.000359 $\pm$ 0.000264	2.30	99.4	125.1	425.44 $\pm$ 4.54
BA6451	19.413 $\pm$ 0.045	0.01255 $\pm$ 0.00077	0.000201 $\pm$ 0.000188	3.38	99.7	34.3	451.48 $\pm$ 2.94
BA6452	19.523 $\pm$ 0.184	0.01791 $\pm$ 0.00297	0.000410 $\pm$ 0.000752	0.73	99.4	24.0	452.50 $\pm$ 11.90
BA6454	19.232 $\pm$ 0.253	0.01069 $\pm$ 0.00380	0.000000 $\pm$ 0.001582	0.49	100.0	40.2	448.95 $\pm$ 10.48
Inverse isochron age $\pm 2\sigma$	447.90 $\pm$ 1.55					Integrated age $\pm 2\sigma$	442.12 $\pm$ 1.88
$^{40}\text{Ar}/^{39}\text{Ar}$ intercept $\pm 2\sigma$	331.9 $\pm$ 64.3		MSWD 1.23		Weighted mean age $\pm 2\sigma$		<b>448.30 <math>\pm</math> 1.36</b>
<b>Rifle Hill bentonite sanidine <math>J = 0.011171 \pm 0.16\%</math> <math>\mu = 1.0030</math></b>							
* AB9350	32.835 $\pm$ 0.113	0.42507 $\pm$ 0.01112	0.053885 $\pm$ 0.013117	0.92	51.6	1.0	312.76 $\pm$ 131.4
AB9418	25.065 $\pm$ 0.064	0.01261 $\pm$ 0.00294	0.000022 $\pm$ 0.000917	1.62	100.0	34.1	445.20 $\pm$ 9.00
* AB9422	46.281 $\pm$ 0.388	2.34360 $\pm$ 0.03578	0.014135 $\pm$ 0.002968	1.36	91.4	0.2	698.90 $\pm$ 26.09
# AB9439	40.336 $\pm$ 0.095	0.00085 $\pm$ 0.00118	0.000494 $\pm$ 0.000391	3.41	99.6	507.9	668.97 $\pm$ 5.04
# AB9442	102.16 $\pm$ 0.306	0.00283 $\pm$ 0.00133	0.002102 $\pm$ 0.000552	8.23	99.4	151.8	1367.66 $\pm$ 8.16
** AB9445	20.312 $\pm$ 0.041	0.00004 $\pm$ 0.00077	0.000587 $\pm$ 0.000219	3.36	99.1	11323	366.00 $\pm$ 3.04
** AB9446	21.572 $\pm$ 0.043	0.00002 $\pm$ 0.00087	0.000303 $\pm$ 0.000214	4.10	99.6	24854	387.98 $\pm$ 3.06
# AB9449	44.661 $\pm$ 0.177	0.00029 $\pm$ 0.00897	0.003063 $\pm$ 0.002704	0.64	98.0	1491	717.90 $\pm$ 22.35
** AB9451	23.988 $\pm$ 0.037	0.00001 $\pm$ 0.00031	0.000577 $\pm$ 0.000094	8.74	99.3	50417	425.53 $\pm$ 2.44
* AB9546	25.116 $\pm$ 0.141	0.00864 $\pm$ 0.00766	0.004425 $\pm$ 0.002959	0.65	94.8	49.8	425.40 $\pm$ 28.24
AB9549	25.190 $\pm$ 0.173	0.03154 $\pm$ 0.00850	0.000814 $\pm$ 0.002425	0.50	99.0	13.6	443.51 $\pm$ 23.32
AB9550	25.536 $\pm$ 0.130	0.00108 $\pm$ 0.00801	0.000441 $\pm$ 0.002756	0.46	99.5	396.8	450.64 $\pm$ 25.98
AB9552	25.183 $\pm$ 0.236	0.00515 $\pm$ 0.00664	0.000409 $\pm$ 0.002549	0.44	99.5	83.6	445.25 $\pm$ 24.93
AB9555	25.970 $\pm$ 0.363	0.00970 $\pm$ 0.01418	0.000164 $\pm$ 0.003607	0.34	99.8	44.3	458.74 $\pm$ 35.25
# AB9556	116.13 $\pm$ 0.464	0.00016 $\pm$ 0.00318	0.000720 $\pm$ 0.001294	4.84	99.8	2663	1498.63 $\pm$ 11.77
* AB9698	27.158 $\pm$ 0.130	0.01648 $\pm$ 0.00632	0.006055 $\pm$ 0.001250	0.98	93.4	26.1	450.09 $\pm$ 12.38
AB9699	25.574 $\pm$ 0.127	0.01240 $\pm$ 0.01034	0.002126 $\pm$ 0.001913	0.57	97.5	34.7	443.42 $\pm$ 18.36
AB9701	26.416 $\pm$ 0.132	0.01864 $\pm$ 0.00619	0.001408 $\pm$ 0.001104	0.90	98.4	23.1	459.97 $\pm$ 11.16
# AB9702	27.824 $\pm$ 0.107	0.01225 $\pm$ 0.00529	0.000895 $\pm$ 0.000866	1.06	99.0	35.1	484.16 $\pm$ 8.81
# AB9811	65.896 $\pm$ 0.541	0.00097 $\pm$ 0.00330	0.000377 $\pm$ 0.000853	3.59	99.8	443.2	993.88 $\pm$ 14.38
* AB9812	43.717 $\pm$ 1.627	0.13454 $\pm$ 0.02000	0.064769 $\pm$ 0.004755	0.51	56.2	3.2	437.81 $\pm$ 50.40
AB9815	25.272 $\pm$ 0.695	0.02158 $\pm$ 0.01364	0.002299 $\pm$ 0.003036	0.44	97.3	19.9	437.86 $\pm$ 35.67
# AB9817	122.26 $\pm$ 1.163	0.00008 $\pm$ 0.00398	0.001226 $\pm$ 0.001107	5.74	99.7	5621	1550.36 $\pm$ 21.24
<b><math>J = 0.010631 \pm 0.20\%</math> <math>\mu = 1.0050</math></b>							
* BB6962	29.001 $\pm$ 0.682	0.01285 $\pm$ 0.00829	0.006157 $\pm$ 0.003599	0.22	93.7	33.5	457.96 $\pm$ 37.54
# BB6963	28.381 $\pm$ 0.084	0.00874 $\pm$ 0.00063	0.000577 $\pm$ 0.000270	3.31	99.4	49.2	473.19 $\pm$ 3.41
BB6965	26.703 $\pm$ 0.094	0.01117 $\pm$ 0.00100	0.000526 $\pm$ 0.000293	2.59	99.4	38.5	448.50 $\pm$ 3.81
BB6966	26.836 $\pm$ 0.328	0.01199 $\pm$ 0.00627	0.001108 $\pm$ 0.001155	0.55	98.8	35.9	447.92 $\pm$ 14.13
BB6970	28.241 $\pm$ 0.803	0.00200 $\pm$ 0.01057	0.003214 $\pm$ 0.004077	0.19	96.6	214.9	459.56 $\pm$ 42.99
# BB6971	208.61 $\pm$ 0.624	0.00121 $\pm$ 0.00124	0.003942 $\pm$ 0.001587	21.27	99.4	355.0	2101.44 $\pm$ 9.31
# BB6973	33.407 $\pm$ 0.255	0.00972 $\pm$ 0.00401	0.001392 $\pm$ 0.001082	0.81	98.8	44.2	542.46 $\pm$ 11.59
# BB6974	159.98 $\pm$ 0.469	0.00471 $\pm$ 0.00239	0.003469 $\pm$ 0.001315	4.92	99.4	91.4	1785.09 $\pm$ 8.66
* BB6976	23.557 $\pm$ 0.259	0.00024 $\pm$ 0.00837	0.006957 $\pm$ 0.002897	0.19	91.3	1757	371.36 $\pm$ 27.77
BB6977	26.997 $\pm$ 0.181	0.00791 $\pm$ 0.00331	0.002831 $\pm$ 0.000842	0.67	96.9	54.4	442.69 $\pm$ 9.15
* BB6979	27.675 $\pm$ 0.395	0.00025 $\pm$ 0.01049	0.007554 $\pm$ 0.004569	0.17	91.9	1724	431.88 $\pm$ 42.24
BB6980	26.980 $\pm$ 0.191	0.00712 $\pm$ 0.00211	0.002359 $\pm$ 0.000737	0.89	97.4	60.4	444.52 $\pm$ 8.61
BB6982	26.990 $\pm$ 0.109	0.00968 $\pm$ 0.00161	0.001796 $\pm$ 0.000534	1.37	98.0	44.4	447.18 $\pm$ 5.71
* BB6983	26.786 $\pm$ 0.157	0.00828 $\pm$ 0.00713	0.005456 $\pm$ 0.002777	0.29	94.0	51.9	427.82 $\pm$ 25.24
# BB6986	167.98 $\pm$ 0.391	0.00081 $\pm$ 0.00087	0.002975 $\pm$ 0.000785	31.42	99.5	529.4	1842.29 $\pm$ 6.26
BB6989	26.777 $\pm$ 0.088	0.01167 $\pm$ 0.00141	0.001429 $\pm$ 0.000442	1.75	98.4	36.8	445.61 $\pm$ 4.69
BB6991	27.205 $\pm$ 0.238	0.01092 $\pm$ 0.00416	0.003476 $\pm$ 0.001374	0.39	96.2	39.4	442.95 $\pm$ 14.00
BB6992	27.015 $\pm$ 0.170	0.00880 $\pm$ 0.00259	0.001664 $\pm$ 0.000531	1.06	98.2	48.8	448.13 $\pm$ 6.88
BB6994	26.762 $\pm$ 0.140	0.01089 $\pm$ 0.00118	0.001432 $\pm$ 0.000490	1.42	98.4	39.5	445.36 $\pm$ 5.99
BB6995	26.748 $\pm$ 0.101	0.00799 $\pm$ 0.00117	0.001554 $\pm$ 0.000688	1.24	98.3	53.8	444.62 $\pm$ 6.78

SUPPLEMENTARY TABLE 1. LASER FUSION  $^{40}\text{Ar}/^{39}\text{Ar}$  RESULTS

Sample Experiment	$^{40}\text{Ar}/^{39}\text{Ar}$	$^{37}\text{Ar}/^{39}\text{Ar}$	$^{36}\text{Ar}/^{39}\text{Ar}$	$^{40}\text{Ar}^*$ X10 <sup>-14</sup> mol	$^{40}\text{Ar}^*$ %	K/Ca	Apparent Age ± 2σ Ma
<b>Rifle Hill bentonite cont...</b>							
BB6997	26.646 ± 0.165	0.00799 ± 0.00484	0.002652 ± 0.001724	0.44	97.1	53.8	438.20 ± 16.06
BB6998	26.457 ± 0.049	0.00713 ± 0.00093	0.001189 ± 0.000239	2.31	98.7	60.3	441.86 ± 2.58
* BB7000	26.743 ± 0.290	0.01790 ± 0.00706	0.003850 ± 0.002344	0.28	95.7	24.0	434.36 ± 22.51
* BB7003	30.171 ± 0.223	0.04520 ± 0.00427	0.012462 ± 0.001701	0.41	87.8	9.5	447.67 ± 16.18
# BB7004	30.499 ± 0.141	0.05031 ± 0.00208	0.002899 ± 0.000918	1.01	97.2	8.5	494.26 ± 8.88
* BB7055	28.743 ± 0.312	0.01655 ± 0.00488	0.005568 ± 0.001614	0.40	94.3	26.0	456.71 ± 16.72
# BB7056	220.52 ± 0.978	0.00215 ± 0.00153	0.002058 ± 0.000466	10.72	99.7	199.7	2174.50 ± 11.32
BB7058	26.841 ± 0.212	0.00750 ± 0.00510	0.001749 ± 0.001348	0.43	98.1	57.3	445.15 ± 13.47
BB7059	27.098 ± 0.108	0.01545 ± 0.00268	0.002113 ± 0.000878	0.75	97.7	27.8	447.39 ± 8.39
BB7061	26.774 ± 0.123	0.01234 ± 0.00144	0.000976 ± 0.000450	1.38	98.9	34.8	447.56 ± 5.39
BB7062	26.449 ± 0.123	0.00657 ± 0.00189	0.000957 ± 0.001029	0.76	98.9	65.4	442.78 ± 9.83
BB7064	26.854 ± 0.153	0.01439 ± 0.00183	0.001004 ± 0.000450	1.14	98.9	29.9	448.65 ± 6.04
BB7065	27.670 ± 0.191	0.00720 ± 0.00334	0.001645 ± 0.001347	0.56	98.2	59.7	457.98 ± 13.10
BB7067	27.331 ± 0.201	0.00597 ± 0.00500	0.001694 ± 0.001528	0.40	98.2	72.0	452.71 ± 14.72
BB7068	28.010 ± 0.279	0.00754 ± 0.01127	0.001657 ± 0.002930	0.20	98.3	57.0	462.98 ± 26.96
BB7070	26.372 ± 0.077	0.00379 ± 0.00167	0.000992 ± 0.000716	1.05	98.9	113.4	441.46 ± 6.76
BB7074	26.865 ± 0.460	0.02073 ± 0.01476	0.000713 ± 0.003062	0.17	99.2	20.7	450.10 ± 30.30
* BB7076	18.261 ± 0.092	0.00451 ± 0.00292	0.001242 ± 0.000976	0.48	98.0	95.4	314.16 ± 9.74
* BB7079	30.582 ± 0.333	0.00518 ± 0.00608	0.003246 ± 0.001953	0.32	96.9	83.1	493.91 ± 19.31
BB7080	26.858 ± 0.084	0.00708 ± 0.00123	0.000801 ± 0.000414	1.70	99.1	60.8	449.60 ± 4.42
BB7082	27.274 ± 0.075	0.00938 ± 0.00143	0.000767 ± 0.000422	1.52	99.2	45.9	455.95 ± 4.32
# BB7083	32.708 ± 0.235	0.01222 ± 0.00915	0.003840 ± 0.002745	0.22	96.5	35.2	522.15 ± 24.21
# BB7085	142.30 ± 0.864	0.00047 ± 0.00377	0.004284 ± 0.001850	2.31	99.1	913.7	1652.56 ± 15.60
BB7086	27.329 ± 0.155	0.00639 ± 0.00592	0.001353 ± 0.001458	0.39	98.5	67.3	454.18 ± 13.64
# BB7088	39.688 ± 0.454	0.00815 ± 0.00626	0.002841 ± 0.002150	0.52	97.9	52.8	623.69 ± 21.06
* BB7089	27.938 ± 0.299	0.00454 ± 0.01063	0.003988 ± 0.003075	0.18	95.8	94.7	451.66 ± 28.47
BB7094	28.355 ± 0.259	0.01111 ± 0.00540	0.001638 ± 0.001659	0.39	98.3	38.7	468.18 ± 16.35
# BB7095	134.91 ± 0.353	0.00036 ± 0.00064	0.001219 ± 0.000238	14.82	99.7	1189	1602.12 ± 5.66
BB7097	26.527 ± 0.076	0.01891 ± 0.00106	0.000928 ± 0.000370	1.97	99.0	22.7	444.09 ± 3.99
** BB7098	14.632 ± 0.069	0.00800 ± 0.00131	0.000975 ± 0.000510	0.73	98.0	53.7	256.05 ± 5.50
BB7100	27.100 ± 0.063	0.00821 ± 0.00077	0.000614 ± 0.000196	2.79	99.3	52.4	454.03 ± 2.54
BB7101	26.876 ± 0.175	0.01296 ± 0.00323	0.001347 ± 0.000750	0.84	98.5	33.2	447.46 ± 8.41
BB7103	26.475 ± 0.129	0.01178 ± 0.00258	0.001183 ± 0.000874	0.79	98.7	36.5	442.16 ± 8.64
BB7104	26.515 ± 0.082	0.00198 ± 0.00269	0.000948 ± 0.000710	0.73	98.9	217.1	443.79 ± 6.75
BB7106	26.536 ± 0.109	0.00839 ± 0.00163	0.001146 ± 0.001033	0.91	98.7	51.3	443.25 ± 9.72
# BB7107	177.59 ± 0.463	0.00672 ± 0.00130	0.002608 ± 0.000814	28.32	99.6	64.0	1908.22 ± 6.93
BB7109	26.636 ± 0.069	0.01091 ± 0.00218	0.001098 ± 0.000522	1.06	98.8	39.4	444.95 ± 5.06
# BB7110	87.410 ± 0.231	0.00150 ± 0.00049	0.000519 ± 0.000112	14.09	99.8	287.2	1183.99 ± 4.63
BB7112	26.524 ± 0.108	0.00646 ± 0.00148	0.000786 ± 0.000686	1.10	99.1	66.5	444.66 ± 6.88
BB7115	26.903 ± 0.106	0.00795 ± 0.00246	0.000982 ± 0.000626	0.94	98.9	54.1	449.47 ± 6.37
# BB7116	137.75 ± 0.506	0.00196 ± 0.00195	0.003135 ± 0.000829	5.32	99.3	219.5	1620.00 ± 8.74
BB7118	29.371 ± 0.306	0.00080 ± 0.01199	0.004022 ± 0.002678	0.20	96.0	538.3	472.77 ± 24.98
BB7119	26.198 ± 0.289	0.01744 ± 0.01361	0.001526 ± 0.002387	0.20	98.3	24.7	436.48 ± 22.94
BB7122	28.539 ± 0.532	0.00061 ± 0.01107	0.002244 ± 0.003494	0.20	97.7	703.8	468.25 ± 34.23
BB7124	26.980 ± 0.126	0.01077 ± 0.00171	0.000960 ± 0.000584	1.18	98.9	39.9	450.72 ± 6.37
BB7125	26.846 ± 0.103	0.01065 ± 0.00139	0.000869 ± 0.000707	1.22	99.0	40.4	449.11 ± 6.96
# BB7131	51.761 ± 0.215	0.01125 ± 0.00177	0.001180 ± 0.000568	1.95	99.3	38.2	786.64 ± 6.73
BB7133	26.555 ± 0.210	0.00825 ± 0.00428	0.001351 ± 0.001164	0.45	98.5	52.1	442.62 ± 12.06
* BB7134	27.774 ± 0.429	0.02853 ± 0.01165	0.003821 ± 0.003655	0.20	95.9	15.1	449.97 ± 34.58
BB7136	27.169 ± 0.225	0.00919 ± 0.00813	0.002368 ± 0.001917	0.26	97.4	46.8	447.32 ± 18.22
BB7137	27.588 ± 0.415	0.01400 ± 0.01427	0.002208 ± 0.004251	0.17	97.6	30.7	454.29 ± 39.39
* BB7139	28.568 ± 0.458	0.00624 ± 0.01308	0.004846 ± 0.002719	0.18	95.0	69.0	457.27 ± 27.28
BB7142	26.663 ± 0.120	0.02117 ± 0.00157	0.000661 ± 0.000422	1.35	99.3	20.3	447.32 ± 5.17
BB7144	26.629 ± 0.114	0.01280 ± 0.00267	0.000937 ± 0.000954	0.88	99.0	33.6	445.58 ± 9.11
BB7145	26.924 ± 0.160	0.00923 ± 0.00352	0.001095 ± 0.001264	0.52	98.8	46.6	449.28 ± 12.14
BB7147	26.732 ± 0.096	0.01277 ± 0.00133	0.000990 ± 0.000564	1.30	98.9	33.7	446.88 ± 5.75
BB7148	27.455 ± 0.123	0.01039 ± 0.00286	0.001285 ± 0.000724	0.75	98.6	41.4	456.37 ± 7.33
BB7150	27.170 ± 0.157	0.01052 ± 0.00444	0.001153 ± 0.001039	0.48	98.7	40.9	452.70 ± 10.28
BB7151	26.734 ± 0.092	0.01676 ± 0.00325	0.000902 ± 0.000850	0.79	99.0	25.7	447.30 ± 8.00
BB7153	26.573 ± 0.110	0.00667 ± 0.00205	0.001138 ± 0.000766	0.84	98.7	64.5	443.82 ± 7.53
BB7154	28.446 ± 0.304	0.00059 ± 0.00869	0.001995 ± 0.002582	0.23	97.9	723.7	467.95 ± 24.26
# BB7156	132.90 ± 0.330	0.00005 ± 0.00055	0.000760 ± 0.000186	17.37	99.8	8421	1587.27 ± 5.32
BB7157	26.791 ± 0.076	0.01104 ± 0.00126	0.000776 ± 0.000463	1.91	99.1	38.9	448.70 ± 4.67

SUPPLEMENTARY TABLE 1. LASER FUSION  $^{40}\text{Ar}/^{39}\text{Ar}$  RESULTS

Sample Experiment	$^{40}\text{Ar}/^{39}\text{Ar}$	$^{37}\text{Ar}/^{39}\text{Ar}$	$^{36}\text{Ar}/^{39}\text{Ar}$	$^{40}\text{Ar}^*$ X10 <sup>-14</sup> mol	$^{40}\text{Ar}^*$ %	K/Ca	Apparent Age ± 2σ Ma
<b>Rifle Hill bentonite cont...</b>							
BB7162	27.089 ± 0.172	0.01362 ± 0.00454	0.001502 ± 0.001152	0.44	98.4	31.6	449.95 ± 11.36
BB7163	27.146 ± 0.210	0.00793 ± 0.00854	0.001694 ± 0.001720	0.29	98.2	54.3	449.96 ± 16.42
BB7168	27.009 ± 0.209	0.01068 ± 0.00439	0.002788 ± 0.001128	0.48	96.9	40.3	443.07 ± 11.73
BB7169	27.727 ± 0.204	0.00551 ± 0.00484	0.002713 ± 0.001609	0.40	97.1	78.0	454.13 ± 15.38
BB7171	28.867 ± 0.441	0.00124 ± 0.01426	0.003110 ± 0.003636	0.16	96.8	347.1	469.31 ± 34.20
BB7172	26.765 ± 0.073	0.00663 ± 0.00250	0.001131 ± 0.000466	1.36	98.7	64.8	446.75 ± 4.66
# BB7174	29.609 ± 0.146	0.00074 ± 0.00541	0.002643 ± 0.001484	0.38	97.4	584.0	482.28 ± 13.53
BB7175	27.174 ± 0.127	0.00805 ± 0.00467	0.001779 ± 0.001108	0.55	98.1	53.4	449.99 ± 10.48
# BB7177	29.585 ± 0.255	0.00329 ± 0.00980	0.003069 ± 0.002499	0.24	96.9	130.8	480.08 ± 22.90
BB7178	27.471 ± 0.154	0.00805 ± 0.00331	0.002090 ± 0.001119	0.56	97.8	53.4	453.06 ± 10.84
BB7180	27.041 ± 0.111	0.00850 ± 0.00544	0.001445 ± 0.001113	0.57	98.4	50.6	449.49 ± 10.36
BB7181	26.937 ± 0.108	0.01100 ± 0.00257	0.001265 ± 0.000807	0.96	98.6	39.1	448.73 ± 7.83
BB7183	27.248 ± 0.180	0.00659 ± 0.00267	0.001873 ± 0.000898	0.75	98.0	65.3	450.69 ± 9.52
BB7187	27.790 ± 0.210	0.01651 ± 0.00687	0.002262 ± 0.001787	0.31	97.6	26.0	457.07 ± 16.87
* BB7189	26.984 ± 0.205	0.00908 ± 0.00613	0.003829 ± 0.002760	0.27	95.8	47.4	438.07 ± 25.24
BB7190	26.935 ± 0.215	0.01881 ± 0.00876	0.001718 ± 0.001824	0.27	98.1	22.9	446.70 ± 17.34
BB7714	27.200 ± 0.194	0.00644 ± 0.00517	0.001418 ± 0.001300	0.44	98.5	66.8	451.98 ± 12.83
BB7716	26.791 ± 0.093	0.00929 ± 0.00189	0.001058 ± 0.000415	1.60	98.8	46.3	447.46 ± 4.59
BB7717	26.848 ± 0.147	0.00399 ± 0.00357	0.000711 ± 0.000730	0.72	99.2	107.7	449.83 ± 7.79
BB7719	27.186 ± 0.514	0.02231 ± 0.01811	0.000353 ± 0.003407	0.15	99.6	19.3	456.48 ± 33.65
BB7720	26.760 ± 0.142	0.01058 ± 0.00221	0.000855 ± 0.000468	1.08	99.1	40.6	447.89 ± 5.91
BB7722	27.098 ± 0.096	0.01219 ± 0.00169	0.001038 ± 0.000494	1.32	98.9	35.3	452.13 ± 5.21
BB7723	28.039 ± 0.399	0.00752 ± 0.00707	0.003654 ± 0.001990	0.30	96.1	57.2	454.64 ± 20.97
BB7725	26.824 ± 0.239	0.00805 ± 0.00456	0.002012 ± 0.001234	0.43	97.8	53.4	443.73 ± 13.02
BB7726	26.159 ± 0.408	0.00800 ± 0.01551	0.002505 ± 0.003599	0.15	97.2	53.7	431.52 ± 34.32
BB7728	26.501 ± 0.133	0.00926 ± 0.00257	0.001264 ± 0.000522	0.96	98.6	46.5	442.19 ± 6.09
BB7731	27.711 ± 0.202	0.00708 ± 0.00666	0.002147 ± 0.001200	0.54	97.7	60.7	456.39 ± 12.11
BB7732	28.213 ± 0.446	0.00497 ± 0.01380	0.002355 ± 0.003012	0.22	97.5	86.6	462.94 ± 29.42
BB7734	26.710 ± 0.253	0.00610 ± 0.00581	0.002367 ± 0.001670	0.41	97.4	70.5	440.44 ± 16.60
BB7735	26.608 ± 0.166	0.01085 ± 0.00365	0.001086 ± 0.000999	0.71	98.8	39.6	444.60 ± 10.13
BB7737	26.892 ± 0.088	0.00761 ± 0.00073	0.001198 ± 0.000294	2.62	98.7	56.5	448.34 ± 3.68
BB7738	26.553 ± 0.298	0.01073 ± 0.00710	0.001954 ± 0.001739	0.36	97.8	40.1	439.91 ± 17.78
BB7741	27.511 ± 0.165	0.00507 ± 0.00668	0.000525 ± 0.001680	0.37	99.4	84.8	460.53 ± 15.55
BB7743	26.821 ± 0.169	0.01469 ± 0.00525	0.001019 ± 0.001475	0.48	98.9	29.3	448.09 ± 13.98
BB7744	26.616 ± 0.202	0.44998 ± 0.01155	0.002219 ± 0.000709	0.76	97.7	1.0	440.33 ± 8.66
BB7746	26.772 ± 0.163	0.01285 ± 0.00378	0.000759 ± 0.000896	0.62	99.2	33.5	448.49 ± 9.29
BB7747	27.476 ± 0.183	0.00746 ± 0.00667	0.001261 ± 0.001680	0.40	98.6	57.6	456.78 ± 15.74
# BB7748	71.709 ± 0.210	0.00375 ± 0.00164	0.001363 ± 0.000478	4.78	99.4	114.8	1017.87 ± 5.50
Inverse isochron age ± 2σ	408.06 ± 12.90					Integrated age ± 2σ	802.73 ± 2.77
$^{40}\text{Ar}/^{39}\text{Ar}$ intercept ± 2σ	2727 ± 3596		MSWD 1.52			Weighted mean age ± 2σ	<b>447.89 ± 1.84</b>

Note: All ages calculated relative to 28.02 Ma for the Fish Canyon tuff sanidine (Renne et al., 1998); using the decay constants of Steiger and Jäger (1977). Uncertainties in Ar isotope ratios reported at 1σ analytical precision, uncertainties in ages reported at 2σ analytical precision. Corrected for  $^{37}\text{Ar}$  and  $^{39}\text{Ar}$  decay, half lives of 35.2 days and 269 years, respectively. Preferred ages are emboldened.

\*Analyses excluded from weighted mean age calculations due to  $^{40}\text{Ar}^* < 96\%$  (see Figure DR1)

# Apparent age excluded from weighted mean age calculations MSWD criteria for older outliers (see text), interpreted to be of xenocrystic or detrital origin.

\*\* Apparent age excluded from weighted mean age calculations based on MSWD criteria for younger outliers (see text), interpreted to incorporate authigenic feldspar and or to have experienced loss of  $^{40}\text{Ar}^*$  due to alteration (see Figure DR1).

**SUPPLEMENTARY TABLE 2. LASER INCREMENTAL HEATING  $^{40}\text{Ar}/^{39}\text{Ar}$  RESULTS**

Sample Experiment	Laser Power (W)	$^{40}\text{Ar}/^{39}\text{Ar}$	$^{37}\text{Ar}/^{39}\text{Ar}$	$^{36}\text{Ar}/^{39}\text{Ar}$	$^{40}\text{Ar}^*$ $\times 10^{-14}$ mol	$^{40}\text{Ar}^*$ %	$^{39}\text{Ar}_K$ %	K/Ca	Apparent Age $\pm 2\sigma$ Ma
<b>Millbrig bentonite sanidine</b> $J = 0.022197 \pm 0.10\%$ $\mu = 1.0025$									
AA4792	1.25	12.686 $\pm$ 0.035	0.00400 $\pm$ 0.00029	0.000058 $\pm$ 0.000115	4.30	99.8	26.8	107.6	446.91 $\pm$ 3.04
AA4795	1.80	12.797 $\pm$ 0.034	0.00480 $\pm$ 0.00016	0.000002 $\pm$ 0.000075	5.94	100.0	36.6	89.7	450.91 $\pm$ 2.54
AA4796	3.00	12.827 $\pm$ 0.032	0.00513 $\pm$ 0.00024	0.000065 $\pm$ 0.000095	5.96	99.8	36.6	83.9	451.26 $\pm$ 2.68
Inverse isochron age $\pm 2\sigma$		459.05 $\pm$ 41.93							Integrated age $\pm 2\sigma$
$^{40}\text{Ar}/^{39}\text{Ar}$ intercept $\pm 2\sigma$		-8710 $\pm$ 1779		MSWD	2.77				Plateau age $\pm 2\sigma$
AA7379	0.16	26.700 $\pm$ 5.494	0.16087 $\pm$ 5.39928	0.043718 $\pm$ 0.075411	0.01	51.6	0.03	2.7	481.81 $\pm$ 1395
AA7380	0.34	15.059 $\pm$ 0.805	0.33231 $\pm$ 0.81091	0.006078 $\pm$ 0.014860	0.05	88.2	0.2	1.3	466.31 $\pm$ 276.0
AA7381	0.59	14.984 $\pm$ 0.543	0.15285 $\pm$ 0.50440	0.004580 $\pm$ 0.007583	0.07	91.0	0.3	2.8	477.14 $\pm$ 141.7
AA7382	0.80	13.482 $\pm$ 0.205	0.00624 $\pm$ 0.20746	0.001834 $\pm$ 0.002823	0.17	95.9	0.9	68.9	455.39 $\pm$ 53.43
AA7384	1.14	12.866 $\pm$ 0.095	0.00144 $\pm$ 0.04382	0.000233 $\pm$ 0.000777	0.71	99.4	3.8	297.7	450.91 $\pm$ 15.50
AA7385	1.48	12.783 $\pm$ 0.086	0.01533 $\pm$ 0.01116	0.000055 $\pm$ 0.000193	2.62	99.8	14.2	28.0	450.00 $\pm$ 6.46
AA7386	1.71	12.820 $\pm$ 0.035	0.00557 $\pm$ 0.00753	0.000137 $\pm$ 0.000091	4.94	99.7	26.8	77.1	450.40 $\pm$ 2.74
AA7388	2.16	12.784 $\pm$ 0.053	0.00198 $\pm$ 0.01571	0.000052 $\pm$ 0.000218	1.95	99.8	10.6	216.7	450.05 $\pm$ 5.23
AA7389	2.62	12.831 $\pm$ 0.038	0.00043 $\pm$ 0.01165	0.000179 $\pm$ 0.000207	2.38	99.6	12.9	1005	450.34 $\pm$ 4.49
AA7390	3.87	12.821 $\pm$ 0.031	0.00706 $\pm$ 0.00630	0.000094 $\pm$ 0.000074	5.10	99.8	27.6	60.9	450.81 $\pm$ 2.36
AA7391	5.00	13.161 $\pm$ 0.101	0.04843 $\pm$ 0.06765	0.000427 $\pm$ 0.000986	0.50	99.0	2.6	8.9	458.44 $\pm$ 19.14
Inverse isochron age $\pm 2\sigma$		449.81 $\pm$ 3.59							Integrated age $\pm 2\sigma$
$^{40}\text{Ar}/^{39}\text{Ar}$ intercept $\pm 2\sigma$		514.6 $\pm$ 890.6		MSWD	0.10				Plateau age $\pm 2\sigma$
AA7627	0.60	13.822 $\pm$ 0.144	0.01388 $\pm$ 0.22099	0.002004 $\pm$ 0.003114	0.19	95.7	0.9	31.0	464.40 $\pm$ 57.66
AA7628	0.75	12.919 $\pm$ 0.069	0.00243 $\pm$ 0.06769	0.000392 $\pm$ 0.000836	0.52	99.1	2.8	177.0	451.10 $\pm$ 15.99
AA7629	0.97	12.803 $\pm$ 0.051	0.00588 $\pm$ 0.01393	0.000079 $\pm$ 0.000180	2.39	99.8	12.9	73.1	450.40 $\pm$ 4.61
AA7631	1.27	12.735 $\pm$ 0.023	0.00032 $\pm$ 0.00442	0.000108 $\pm$ 0.000067	7.03	99.7	38.0	1353	447.98 $\pm$ 1.89
AA7632	1.50	12.815 $\pm$ 0.038	0.00070 $\pm$ 0.01246	0.000087 $\pm$ 0.000134	3.13	99.8	16.8	613.4	450.68 $\pm$ 3.42
AA7633	2.10	12.810 $\pm$ 0.027	0.00046 $\pm$ 0.00949	0.000109 $\pm$ 0.000126	3.99	99.7	21.4	938.1	450.31 $\pm$ 2.88
AA7635	2.70	13.019 $\pm$ 0.037	0.00129 $\pm$ 0.02162	0.000148 $\pm$ 0.000381	1.37	99.6	7.2	334.6	456.46 $\pm$ 7.36
Inverse isochron age $\pm 2\sigma$		436.25 $\pm$ 38.85							Integrated age $\pm 2\sigma$
$^{40}\text{Ar}/^{39}\text{Ar}$ intercept $\pm 2\sigma$		4223 $\pm$ 34119		MSWD	1.23				Plateau age $\pm 2\sigma$
AA7757	0.75	16.203 $\pm$ 0.293	0.16951 $\pm$ 0.59210	0.008051 $\pm$ 0.005846	0.10	85.4	0.4	2.5	483.13 $\pm$ 107.1
AA7758	1.05	13.529 $\pm$ 0.077	0.00639 $\pm$ 0.15623	0.001256 $\pm$ 0.001261	0.26	97.2	1.2	67.3	462.16 $\pm$ 23.60
AA7759	1.65	12.806 $\pm$ 0.023	0.00454 $\pm$ 0.01245	0.000080 $\pm$ 0.000095	4.57	99.8	22.7	94.7	450.48 $\pm$ 2.26
AA7761	2.40	12.829 $\pm$ 0.028	0.00027 $\pm$ 0.00301	0.000080 $\pm$ 0.000034	12.99	99.8	64.3	1592	451.19 $\pm$ 1.83
AA7762	3.00	12.846 $\pm$ 0.035	0.00142 $\pm$ 0.01883	0.000178 $\pm$ 0.000151	2.30	99.6	11.4	303.3	450.81 $\pm$ 3.54
Inverse isochron age $\pm 2\sigma$		450.43 $\pm$ 2.45							Integrated age $\pm 2\sigma$
$^{40}\text{Ar}/^{39}\text{Ar}$ intercept $\pm 2\sigma$		493.6 $\pm$ 587.8		MSWD	0.38				Plateau age $\pm 2\sigma$
AA7775	1.00	12.814 $\pm$ 0.042	0.00041 $\pm$ 0.01038	0.000300 $\pm$ 0.000105	3.98	99.3	16.1	1052	448.69 $\pm$ 3.26
AA7776	1.50	12.827 $\pm$ 0.029	0.00334 $\pm$ 0.01175	0.000192 $\pm$ 0.000120	3.64	99.5	14.7	128.7	450.10 $\pm$ 2.85
AA7777	2.00	12.820 $\pm$ 0.023	0.00605 $\pm$ 0.00486	0.000150 $\pm$ 0.000064	7.51	99.6	30.4	71.0	450.26 $\pm$ 1.88
AA7779	2.50	12.865 $\pm$ 0.038	0.00970 $\pm$ 0.00992	0.000149 $\pm$ 0.000105	4.19	99.6	16.9	44.3	451.67 $\pm$ 3.08
AA7780	3.00	12.803 $\pm$ 0.024	0.00703 $\pm$ 0.00849	0.000062 $\pm$ 0.000080	5.41	99.8	21.9	61.2	450.56 $\pm$ 2.09
Inverse isochron age $\pm 2\sigma$		451.06 $\pm$ 2.18							Integrated age $\pm 2\sigma$
$^{40}\text{Ar}/^{39}\text{Ar}$ intercept $\pm 2\sigma$		136.0 $\pm$ 211.2		MSWD	0.46				Plateau age $\pm 2\sigma$

**SUPPLEMENTARY TABLE 2. LASER INCREMENTAL HEATING  $^{40}\text{Ar}/^{39}\text{Ar}$  RESULTS**

Sample Experiment	Laser Power (W)	$^{40}\text{Ar}/^{39}\text{Ar}$	$^{37}\text{Ar}/^{39}\text{Ar}$	$^{36}\text{Ar}/^{39}\text{Ar}$	$^{40}\text{Ar}^*$ $\times 10^{-14}$ mol	$^{40}\text{Ar}^*$ %	$^{39}\text{Ar}_K$ %	K/Ca	Apparent Age $\pm 2\sigma$ Ma
<b>Dygerts bentonite sanidine</b> $J = 0.009615 \pm 0.17\%$ $\mu = 1.0025$									
BB3407	0.75	29.783 $\pm$ 0.061	0.31883 $\pm$ 0.00459	0.003789 $\pm$ 0.000187	9.94	96.3	55.3	1.3	439.54 $\pm$ 2.21
BB3408	1.05	29.191 $\pm$ 0.065	0.11334 $\pm$ 0.00201	0.000671 $\pm$ 0.000144	5.55	99.3	31.6	3.8	443.76 $\pm$ 2.09
BB3410	1.65	29.548 $\pm$ 0.110	0.01790 $\pm$ 0.00275	0.001014 $\pm$ 0.000530	1.40	99.0	7.9	24.0	447.09 $\pm$ 5.18
BB3411	2.40	26.373 $\pm$ 0.187	0.01678 $\pm$ 0.00817	0.001189 $\pm$ 0.002372	0.37	98.7	2.3	25.6	402.86 $\pm$ 20.12
BB3413	3.00	14.797 $\pm$ 0.157	0.00951 $\pm$ 0.00581	0.000549 $\pm$ 0.002086	0.26	98.9	3.0	45.2	237.52 $\pm$ 19.34
No plateau age					Integrated age $\pm 2\sigma$				434.97 $\pm$ 2.08
BB3416	0.53	54.176 $\pm$ 0.721	0.44800 $\pm$ 0.03296	0.002187 $\pm$ 0.003855	0.35	98.9	1.9	1.0	749.64 $\pm$ 30.78
BB3418	0.75	30.173 $\pm$ 0.046	0.08338 $\pm$ 0.00152	0.000382 $\pm$ 0.000126	7.70	99.6	73.2	5.2	458.13 $\pm$ 1.58
BB3419	1.05	29.692 $\pm$ 0.118	0.01564 $\pm$ 0.00268	0.001200 $\pm$ 0.000633	1.70	98.8	16.5	27.5	448.30 $\pm$ 5.96
BB3421	1.35	30.034 $\pm$ 0.375	0.02132 $\pm$ 0.00543	0.001274 $\pm$ 0.002135	0.55	98.7	5.2	20.2	452.63 $\pm$ 19.76
BB3422	3.00	34.387 $\pm$ 0.416	0.06048 $\pm$ 0.01150	0.001925 $\pm$ 0.003535	0.38	98.4	3.2	7.1	507.98 $\pm$ 29.38
No plateau age					Integrated age $\pm 2\sigma$				463.73 $\pm$ 2.57
BB3424	0.60	30.296 $\pm$ 0.370	0.00531 $\pm$ 0.00777	0.002908 $\pm$ 0.001698	0.54	97.2	5.6	81.0	449.61 $\pm$ 16.73
BB3425	0.75	29.476 $\pm$ 0.056	0.01267 $\pm$ 0.00202	0.000640 $\pm$ 0.000370	2.58	99.4	27.5	33.9	447.61 $\pm$ 3.32
BB3429	3.00	29.174 $\pm$ 0.077	0.01104 $\pm$ 0.00068	0.000535 $\pm$ 0.000129	6.21	99.5	66.9	39.0	443.93 $\pm$ 2.33
Inverse isochron age $\pm 2\sigma$		440.02 $\pm$ 10.44				Integrated age $\pm 2\sigma$		445.26 $\pm$ 2.44	
$^{40}\text{Ar}/^{39}\text{Ar}$ intercept $\pm 2\sigma$		881.9 $\pm$ 1611		MSWD 1.78		Plateau age $\pm 2\sigma$		445.20 $\pm$ 2.86	
BB3431	0.60	31.537 $\pm$ 0.430	2.16327 $\pm$ 0.05702	0.016686 $\pm$ 0.003135	0.24	84.9	3.1	0.2	413.80 $\pm$ 27.57
BB3432	0.75	29.295 $\pm$ 0.105	0.30902 $\pm$ 0.00596	0.001320 $\pm$ 0.000787	1.28	98.7	18.1	1.4	442.81 $\pm$ 6.91
BB3433	1.13	29.197 $\pm$ 0.088	0.01283 $\pm$ 0.00066	0.000582 $\pm$ 0.000217	4.95	99.4	70.3	33.5	444.05 $\pm$ 2.95
BB3435	1.80	29.496 $\pm$ 0.212	0.02734 $\pm$ 0.00737	0.002159 $\pm$ 0.001697	0.54	97.8	7.6	15.7	441.81 $\pm$ 14.74
BB3436	3.00	32.115 $\pm$ 0.983	0.20929 $\pm$ 0.07073	0.014213 $\pm$ 0.012913	0.07	87.0	0.9	2.1	429.20 $\pm$ 107.2
Inverse isochron age $\pm 2\sigma$		445.15 $\pm$ 2.78				Integrated age $\pm 2\sigma$		442.60 $\pm$ 3.25	
$^{40}\text{Ar}/^{39}\text{Ar}$ intercept $\pm 2\sigma$		158.9 $\pm$ 80.2		MSWD 1.26		Plateau age $\pm 2\sigma$		443.50 $\pm$ 3.26	
BB3438	0.60	36.318 $\pm$ 0.364	5.58868 $\pm$ 0.10043	0.057173 $\pm$ 0.002043	0.45	54.7	5.1	0.1	316.33 $\pm$ 18.46
BB3439	0.75	29.793 $\pm$ 0.200	1.38465 $\pm$ 0.02167	0.002328 $\pm$ 0.000759	1.16	98.1	16.0	0.3	446.96 $\pm$ 8.08
BB3440	1.13	29.363 $\pm$ 0.107	0.02000 $\pm$ 0.00140	0.000850 $\pm$ 0.000301	2.78	99.1	39.3	21.5	445.25 $\pm$ 3.76
BB3442	1.80	29.344 $\pm$ 0.098	0.01950 $\pm$ 0.00179	0.000619 $\pm$ 0.000416	2.26	99.4	31.8	22.1	445.91 $\pm$ 4.26
BB3443	3.00	28.744 $\pm$ 0.148	0.06186 $\pm$ 0.00668	0.008451 $\pm$ 0.001766	0.53	91.3	7.7	7.0	406.05 $\pm$ 14.99
No plateau age					Integrated age $\pm 2\sigma$				436.35 $\pm$ 3.09
BB3445	0.60	37.351 $\pm$ 0.393	2.37176 $\pm$ 0.04466	0.051575 $\pm$ 0.002823	0.39	59.7	7.0	0.2	350.89 $\pm$ 24.76
BB3446	0.75	30.119 $\pm$ 0.155	0.76523 $\pm$ 0.01485	0.002875 $\pm$ 0.001549	0.58	97.4	12.9	0.6	448.37 $\pm$ 13.06
BB3447	1.13	29.883 $\pm$ 0.203	1.87717 $\pm$ 0.03014	0.002532 $\pm$ 0.001330	0.54	98.0	12.0	0.2	448.01 $\pm$ 11.95
BB3449	1.80	28.853 $\pm$ 0.116	0.30881 $\pm$ 0.00738	0.001378 $\pm$ 0.001254	0.71	98.7	16.4	1.4	436.58 $\pm$ 10.57
BB3450	3.00	29.299 $\pm$ 0.101	0.01543 $\pm$ 0.00166	0.001112 $\pm$ 0.000299	2.28	98.9	51.8	27.9	443.32 $\pm$ 3.62
No plateau age					Integrated age $\pm 2\sigma$				437.16 $\pm$ 3.99
BB3452	0.60	39.992 $\pm$ 0.346	6.41780 $\pm$ 0.12309	0.109821 $\pm$ 0.004487	0.38	20.1	3.4	0.1	134.89 $\pm$ 42.27
BB3453	0.75	30.649 $\pm$ 0.356	8.68176 $\pm$ 0.16637	0.014774 $\pm$ 0.004063	0.21	88.0	2.5	0.0	418.00 $\pm$ 34.36
BB3454	1.13	29.433 $\pm$ 0.096	0.09786 $\pm$ 0.00319	0.001026 $\pm$ 0.000580	1.27	99.0	15.5	4.4	445.59 $\pm$ 5.31
BB3456	1.80	29.168 $\pm$ 0.078	0.01178 $\pm$ 0.00071	0.000241 $\pm$ 0.000105	6.12	99.8	75.5	36.5	445.03 $\pm$ 2.28
BB3457	3.00	25.977 $\pm$ 0.557	0.00024 $\pm$ 0.02018	0.000847 $\pm$ 0.002914	0.23	99.0	3.1	1781	398.74 $\pm$ 28.45
No plateau age					Integrated age $\pm 2\sigma$				433.26 $\pm$ 2.89

**SUPPLEMENTARY TABLE 2. LASER INCREMENTAL HEATING  $^{40}\text{Ar}/^{39}\text{Ar}$  RESULTS**

Sample Experiment	Laser Power (W)	$^{40}\text{Ar}/^{39}\text{Ar}$	$^{37}\text{Ar}/^{39}\text{Ar}$	$^{36}\text{Ar}/^{39}\text{Ar}$	$^{40}\text{Ar}^*$ $\times 10^{-14}$ mol	$^{40}\text{Ar}^*$ %	$^{39}\text{Ar}_K$ %	K/Ca	Apparent Age $\pm 2\sigma$ Ma
<b>Dygerts bentonite cont...</b>									
BB3459	0.60	29.884 $\pm$ 0.433	0.00617 $\pm$ 0.01520	0.000405 $\pm$ 0.003288	0.29	99.6	5.1	69.7	454.05 $\pm$ 28.68
BB3460	0.75	29.243 $\pm$ 0.136	0.00831 $\pm$ 0.00437	0.000663 $\pm$ 0.001311	0.92	99.3	16.8	51.7	444.35 $\pm$ 11.13
BB3461	1.13	29.246 $\pm$ 0.118	0.01080 $\pm$ 0.00181	0.000654 $\pm$ 0.000298	2.36	99.3	42.9	39.8	444.43 $\pm$ 3.98
BB3463	1.80	29.269 $\pm$ 0.111	0.00913 $\pm$ 0.00255	0.000599 $\pm$ 0.000342	1.81	99.4	33.0	47.1	444.96 $\pm$ 4.05
BB3464	3.00	27.597 $\pm$ 0.619	0.03501 $\pm$ 0.03444	0.008208 $\pm$ 0.006869	0.11	91.2	2.1	12.3	391.05 $\pm$ 59.02
Inverse isochron age $\pm 2\sigma$		449.93 $\pm$ 6.02				Integrated age $\pm 2\sigma$			443.98 $\pm$ 3.70
$^{40}\text{Ar}/^{39}\text{Ar}$ intercept $\pm 2\sigma$		-314.2 $\pm$ 673.4		MSWD 0.97		Plateau age $\pm 2\sigma$			444.63 $\pm$ 3.05
BB3466	0.60	35.094 $\pm$ 0.101	1.20308 $\pm$ 0.01888	0.022711 $\pm$ 0.000468	2.25	81.1	21.8	0.4	436.90 $\pm$ 4.42
BB3467	0.75	29.206 $\pm$ 0.071	0.01960 $\pm$ 0.00082	0.000495 $\pm$ 0.000152	6.48	99.5	75.6	21.9	444.54 $\pm$ 2.28
BB3468	1.13	31.816 $\pm$ 0.787	0.14146 $\pm$ 0.04115	0.003487 $\pm$ 0.008106	0.12	96.8	1.3	3.0	467.95 $\pm$ 67.32
BB3470	1.80	31.890 $\pm$ 0.847	0.02329 $\pm$ 0.11377	0.005443 $\pm$ 0.016482	0.07	95.0	0.7	18.5	461.03 $\pm$ 133
BB3471	3.00	25.258 $\pm$ 1.338	0.00542 $\pm$ 0.08417	0.016456 $\pm$ 0.022385	0.04	80.7	0.5	79.3	323.05 $\pm$ 194.5
No plateau age					Integrated age $\pm 2\sigma$			442.71 $\pm$ 2.89	
BB3473	0.60	29.735 $\pm$ 0.142	0.00839 $\pm$ 0.00371	0.001491 $\pm$ 0.001043	1.13	98.5	7.7	51.2	447.70 $\pm$ 9.17
BB3474	0.75	29.256 $\pm$ 0.050	0.01002 $\pm$ 0.00065	0.000298 $\pm$ 0.000114	7.26	99.7	50.4	42.9	446.00 $\pm$ 1.64
BB3475	1.13	29.363 $\pm$ 0.055	0.01148 $\pm$ 0.00088	0.000110 $\pm$ 0.000147	5.52	99.9	38.2	37.5	448.20 $\pm$ 1.89
BB3477	1.80	29.896 $\pm$ 0.259	0.00510 $\pm$ 0.01224	0.002237 $\pm$ 0.002999	0.33	97.8	2.2	84.3	446.89 $\pm$ 24.97
BB3478	3.00	22.392 $\pm$ 0.368	0.06722 $\pm$ 0.01914	0.005094 $\pm$ 0.003301	0.16	93.3	1.5	6.4	330.25 $\pm$ 29.97
No plateau age					Integrated age $\pm 2\sigma$			445.32 $\pm$ 2.00	
BB3480	0.60	31.001 $\pm$ 0.412	3.73007 $\pm$ 0.07462	0.017104 $\pm$ 0.002917	0.32	84.6	2.3	0.1	406.75 $\pm$ 25.93
BB3481	0.75	29.392 $\pm$ 0.127	0.30429 $\pm$ 0.00618	0.001012 $\pm$ 0.000526	1.52	99.1	11.5	1.4	445.37 $\pm$ 5.42
BB3482	1.13	29.077 $\pm$ 0.057	0.01030 $\pm$ 0.00057	0.000457 $\pm$ 0.000114	8.44	99.5	64.9	41.7	442.93 $\pm$ 1.80
BB3484	1.80	29.831 $\pm$ 0.153	0.00492 $\pm$ 0.00615	0.000912 $\pm$ 0.000993	0.72	99.1	5.4	87.4	451.31 $\pm$ 8.93
BB3485	3.00	28.214 $\pm$ 0.071	0.01046 $\pm$ 0.00304	0.001011 $\pm$ 0.000439	2.01	98.9	15.9	41.1	428.95 $\pm$ 4.04
No plateau age					Integrated age $\pm 2\sigma$			440.63 $\pm$ 2.12	

**SUPPLEMENTARY TABLE 2. LASER INCREMENTAL HEATING  $^{40}\text{Ar}/^{39}\text{Ar}$  RESULTS**

Sample Experiment	Laser Power (W)	$^{40}\text{Ar}/^{39}\text{Ar}$	$^{37}\text{Ar}/^{39}\text{Ar}$	$^{36}\text{Ar}/^{39}\text{Ar}$	$^{40}\text{Ar}^*$ $\times 10^{-14}$ mol	$^{40}\text{Ar}^*$ %	$^{39}\text{Ar}_K$ %	K/Ca	Apparent Age $\pm 2\sigma$ Ma	
<b>Rifle Hill bentonite sanidine</b> $J = 0.010631 \pm 0.20\%$ $\mu = 1.0050$										
BB7333	0.38	27.608 $\pm$ 0.523	0.00081 $\pm$ 0.02170	0.001299 $\pm$ 0.004563	0.12	98.6	8.4	532.5	458.57 $\pm$ 42.95	
BB7334	0.60	26.902 $\pm$ 0.149	0.01179 $\pm$ 0.00313	0.000564 $\pm$ 0.000660	0.82	99.4	58.3	36.5	451.30 $\pm$ 7.31	
BB7336	1.05	31.438 $\pm$ 0.192	0.01707 $\pm$ 0.00592	0.001846 $\pm$ 0.001862	0.51	98.3	30.9	25.2	512.35 $\pm$ 16.79	
BB7337	3.00	30.288 $\pm$ 1.960	0.05237 $\pm$ 0.07023	0.007070 $\pm$ 0.019492	0.04	93.1	2.4	8.2	473.09 $\pm$ 178.3	
No plateau age									Integrated age $\pm 2\sigma$	471.51 $\pm$ 8.94
BB7339	0.38	26.550 $\pm$ 0.284	0.00558 $\pm$ 0.01767	0.000785 $\pm$ 0.003538	0.15	99.1	9.5	77.1	445.05 $\pm$ 32.46	
BB7340	0.53	26.906 $\pm$ 0.095	0.01083 $\pm$ 0.00225	0.001109 $\pm$ 0.000823	0.98	98.8	59.6	39.7	448.95 $\pm$ 7.80	
BB7341	0.75	27.176 $\pm$ 0.228	0.00597 $\pm$ 0.00588	0.001291 $\pm$ 0.002013	0.32	98.6	19.2	72.0	452.17 $\pm$ 18.99	
BB7343	1.05	27.269 $\pm$ 0.388	0.00569 $\pm$ 0.01954	0.000541 $\pm$ 0.004559	0.12	99.4	7.0	75.5	456.87 $\pm$ 41.72	
BB7344	3.00	27.742 $\pm$ 0.589	0.00658 $\pm$ 0.03109	0.001366 $\pm$ 0.007189	0.08	98.5	4.7	65.4	460.27 $\pm$ 65.47	
Inverse isochron age $\pm 2\sigma$		406.67 $\pm$ 480.32				Integrated age $\pm 2\sigma$		450.29 $\pm$ 8.06		
$^{40}\text{Ar}/^{39}\text{Ar}$ intercept $\pm 2\sigma$		2860 $\pm$ 77050		MSWD 0.10		Plateau age $\pm 2\sigma$		449.54 $\pm$ 7.08		
BB7346	0.38	28.048 $\pm$ 0.763	0.00522 $\pm$ 0.01440	0.000059 $\pm$ 0.003441	0.16	99.9	23.1	82.3	470.53 $\pm$ 37.56	
BB7347	0.53	28.807 $\pm$ 0.403	0.01445 $\pm$ 0.01395	0.002256 $\pm$ 0.002402	0.23	97.7	31.5	29.8	472.17 $\pm$ 23.98	
BB7348	0.75	27.789 $\pm$ 0.414	0.02743 $\pm$ 0.01181	0.002556 $\pm$ 0.002958	0.19	97.3	27.3	15.7	455.78 $\pm$ 28.69	
BB7350	1.05	27.808 $\pm$ 0.707	0.03217 $\pm$ 0.04654	0.004035 $\pm$ 0.008262	0.06	95.7	9.2	13.4	449.53 $\pm$ 75.87	
BB7351	3.00	26.493 $\pm$ 0.660	0.01219 $\pm$ 0.04858	0.007560 $\pm$ 0.010608	0.06	91.6	8.9	35.3	413.93 $\pm$ 97.59	
Inverse isochron age $\pm 2\sigma$		510.11 $\pm$ 111.11				Integrated age $\pm 2\sigma$		460.12 $\pm$ 17.79		
$^{40}\text{Ar}/^{39}\text{Ar}$ intercept $\pm 2\sigma$		-1198 $\pm$ 8653		MSWD 0.54		Plateau age $\pm 2\sigma$		464.16 $\pm$ 16.01		
BB7353	0.38	29.691 $\pm$ 0.373	0.00397 $\pm$ 0.00827	0.000737 $\pm$ 0.004407	0.32	99.3	54.6	108.2	491.73 $\pm$ 39.56	
BB7354	0.53	37.752 $\pm$ 0.525	0.00005 $\pm$ 0.00946	0.001098 $\pm$ 0.005373	0.31	99.1	42.3	8000	604.29 $\pm$ 45.87	
BB7355	0.75	48.767 $\pm$ 7.606	0.04699 $\pm$ 0.14248	0.027122 $\pm$ 0.088410	0.02	83.6	2.4	9.2	649.40 $\pm$ 726.2	
BB7357	1.05	40.487 $\pm$ 133.28	0.22763 $\pm$ 2.45494	0.041056 $\pm$ 1.802371	0.001	70.1	0.1	1.9	475.64 $\pm$ 16129	
BB7358	3.00	16.697 $\pm$ 32.178	1.13820 $\pm$ 0.66511	0.010672 $\pm$ 0.455871	0.002	81.6	0.5	0.4	244.33 $\pm$ 4642	
No plateau age									Integrated age $\pm 2\sigma$	542.93 $\pm$ 45.33
BB7360	0.38	27.306 $\pm$ 0.438	0.00042 $\pm$ 0.00849	0.001683 $\pm$ 0.003261	0.24	98.2	18.4	1023	452.37 $\pm$ 31.58	
BB7361	0.53	26.888 $\pm$ 0.237	0.00675 $\pm$ 0.00229	0.001325 $\pm$ 0.000962	0.83	98.5	64.1	63.7	447.73 $\pm$ 11.03	
BB7362	0.75	27.219 $\pm$ 0.594	0.00881 $\pm$ 0.01224	0.000671 $\pm$ 0.004002	0.19	99.3	14.4	48.8	455.56 $\pm$ 39.41	
BB7364	1.05	25.994 $\pm$ 3.829	0.08038 $\pm$ 0.08927	0.002451 $\pm$ 0.032841	0.02	97.2	1.9	5.3	429.38 $\pm$ 315.4	
BB7365	3.00	25.226 $\pm$ 6.507	0.04244 $\pm$ 0.11518	0.014346 $\pm$ 0.056697	0.01	83.2	1.1	10.1	363.38 $\pm$ 563.3	
Inverse isochron age $\pm 2\sigma$		513.78 $\pm$ 450.36				Integrated age $\pm 2\sigma$		448.44 $\pm$ 13.83		
$^{40}\text{Ar}/^{39}\text{Ar}$ intercept $\pm 2\sigma$		-3070 $\pm$ 127148		MSWD 0.08		Plateau age $\pm 2\sigma$		448.66 $\pm$ 10.18		
BB7367	0.38	27.208 $\pm$ 0.221	0.01498 $\pm$ 0.00804	0.003148 $\pm$ 0.002050	0.28	96.6	15.1	28.7	444.46 $\pm$ 19.27	
BB7368	0.53	26.661 $\pm$ 0.127	0.01288 $\pm$ 0.00171	0.001124 $\pm$ 0.000454	1.33	98.8	72.2	33.4	445.22 $\pm$ 5.52	
BB7369	0.75	27.658 $\pm$ 0.255	0.02685 $\pm$ 0.01338	0.000256 $\pm$ 0.002670	0.16	99.7	8.5	16.0	463.94 $\pm$ 24.59	
BB7371	1.05	28.826 $\pm$ 0.718	0.00879 $\pm$ 0.03349	0.001686 $\pm$ 0.008820	0.06	98.3	3.0	48.9	474.93 $\pm$ 79.62	
BB7372	3.00	25.777 $\pm$ 1.565	0.11080 $\pm$ 0.07660	0.004330 $\pm$ 0.032465	0.02	95.1	1.2	3.9	417.71 $\pm$ 295.6	
Inverse isochron age $\pm 2\sigma$		418.01 $\pm$ 63.81				Integrated age $\pm 2\sigma$		447.28 $\pm$ 7.03		
$^{40}\text{Ar}/^{39}\text{Ar}$ intercept $\pm 2\sigma$		1838 $\pm$ 13406		MSWD 0.69		Plateau age $\pm 2\sigma$		446.10 $\pm$ 5.41		
BB7374	0.38	28.258 $\pm$ 0.128	0.00280 $\pm$ 0.00397	0.001220 $\pm$ 0.001062	0.63	98.7	36.9	153.7	468.56 $\pm$ 10.01	
BB7375	0.53	28.126 $\pm$ 0.157	0.01243 $\pm$ 0.00237	0.000917 $\pm$ 0.000641	0.80	99.0	47.6	34.6	467.94 $\pm$ 7.25	
BB7376	0.75	27.331 $\pm$ 0.258	0.02778 $\pm$ 0.01209	0.001512 $\pm$ 0.003243	0.22	98.4	13.1	15.5	453.54 $\pm$ 29.58	
BB7378	1.05	27.412 $\pm$ 1.766	0.03276 $\pm$ 0.09636	0.001856 $\pm$ 0.037040	0.02	98.0	1.2	13.1	453.24 $\pm$ 330.7	
BB7379	3.00	33.457 $\pm$ 2.270	0.01873 $\pm$ 0.09023	0.013835 $\pm$ 0.034034	0.02	87.8	1.1	23.0	490.22 $\pm$ 300.0	
Inverse isochron age $\pm 2\sigma$		439.76 $\pm$ 131.6				Integrated age $\pm 2\sigma$		466.35 $\pm$ 8.39		
$^{40}\text{Ar}/^{39}\text{Ar}$ intercept $\pm 2\sigma$		2144 $\pm$ 29136		MSWD 0.25		Plateau age $\pm 2\sigma$		467.60 $\pm$ 5.99		

**SUPPLEMENTARY TABLE 2. LASER INCREMENTAL HEATING  $^{40}\text{Ar}/^{39}\text{Ar}$  RESULTS**

Sample Experiment	Laser Power (W)	$^{40}\text{Ar}/^{39}\text{Ar}$	$^{37}\text{Ar}/^{39}\text{Ar}$	$^{36}\text{Ar}/^{39}\text{Ar}$	$^{40}\text{Ar}^*$ $\times 10^{-14}$ mol	$^{40}\text{Ar}^*$ %	$^{39}\text{Ar}_K$ %	K/Ca	Apparent Age $\pm 2\sigma$ Ma
<b>Rifle Hill bentonite cont...</b>									
BB7381	0.38	28.230 $\pm$ 0.156	0.00280 $\pm$ 0.00256	0.001215 $\pm$ 0.000982	0.73	98.7	27.9	153.6	468.17 $\pm$ 9.72
BB7382	0.53	27.330 $\pm$ 0.137	0.00739 $\pm$ 0.00175	0.001176 $\pm$ 0.000619	1.49	98.7	59.0	58.2	454.98 $\pm$ 6.78
BB7383	0.75	33.034 $\pm$ 0.353	0.01304 $\pm$ 0.00736	0.004593 $\pm$ 0.002114	0.35	95.9	11.3	33.0	523.63 $\pm$ 20.40
BB7385	1.05	27.568 $\pm$ 0.959	0.06807 $\pm$ 0.05388	0.000550 $\pm$ 0.021122	0.04	99.4	1.4	6.3	461.36 $\pm$ 187.6
BB7386	3.00	34.860 $\pm$ 2.568	0.09550 $\pm$ 0.20747	0.028030 $\pm$ 0.062527	0.01	76.3	0.4	4.5	449.05 $\pm$ 555.9
No plateau age					Integrated age $\pm 2\sigma$				466.60 $\pm$ 6.64
BB7388	0.38	27.663 $\pm$ 0.319	0.00219 $\pm$ 0.01283	0.000207 $\pm$ 0.002727	0.18	99.8	41.7	196.2	464.19 $\pm$ 25.70
BB7389	0.53	28.178 $\pm$ 0.409	0.01242 $\pm$ 0.01349	0.002416 $\pm$ 0.003296	0.17	97.5	38.9	34.6	462.15 $\pm$ 31.25
BB7390	0.75	28.105 $\pm$ 0.518	0.00611 $\pm$ 0.02511	0.002855 $\pm$ 0.006680	0.08	97.0	17.8	70.4	459.14 $\pm$ 60.60
BB7392	1.05	31.883 $\pm$ 6.085	0.09115 $\pm$ 0.42207	0.008221 $\pm$ 0.096566	0.01	92.4	1.4	4.7	491.56 $\pm$ 849.7
BB7393	3.00	60.478 $\pm$ 52.383	1.82833 $\pm$ 2.66139	0.046169 $\pm$ 0.458604	0.002	77.7	0.2	0.2	731.52 $\pm$ 3615
Inverse isochron age $\pm 2\sigma$		463.25 $\pm$ 26.52						Integrated age $\pm 2\sigma$	
$^{40}\text{Ar}/^{39}\text{Ar}$ intercept $\pm 2\sigma$		280.7 $\pm$ 1118		MSWD 0.01				Plateau age $\pm 2\sigma$	
BB7395	0.38	27.748 $\pm$ 0.196	0.00614 $\pm$ 0.00614	0.002090 $\pm$ 0.001681	0.34	97.8	28.6	70.0	457.18 $\pm$ 15.86
BB7396	0.53	26.745 $\pm$ 0.124	0.00750 $\pm$ 0.00590	0.001301 $\pm$ 0.000880	0.62	98.6	54.8	57.3	445.69 $\pm$ 8.61
BB7397	0.75	27.286 $\pm$ 0.597	0.03632 $\pm$ 0.02903	0.005263 $\pm$ 0.007719	0.08	94.3	6.5	11.8	436.27 $\pm$ 70.78
BB7399	1.05	28.631 $\pm$ 0.725	0.02490 $\pm$ 0.04671	0.004899 $\pm$ 0.008687	0.06	94.9	4.8	17.3	457.99 $\pm$ 79.10
BB7400	3.00	27.556 $\pm$ 0.572	0.00749 $\pm$ 0.03824	0.000143 $\pm$ 0.009154	0.06	99.8	5.3	57.4	462.88 $\pm$ 82.05
Inverse isochron age $\pm 2\sigma$		430.99 $\pm$ 65.85						Integrated age $\pm 2\sigma$	
$^{40}\text{Ar}/^{39}\text{Ar}$ intercept $\pm 2\sigma$		1048 $\pm$ 3896		MSWD 0.48				Plateau age $\pm 2\sigma$	
BB7402	0.38	27.115 $\pm$ 0.310	0.00684 $\pm$ 0.01076	0.000195 $\pm$ 0.002655	0.18	99.8	17.2	62.9	456.10 $\pm$ 25.12
BB7403	0.53	27.153 $\pm$ 0.183	0.00756 $\pm$ 0.00351	0.001605 $\pm$ 0.001171	0.47	98.3	44.7	56.9	450.45 $\pm$ 11.66
BB7404	0.75	27.575 $\pm$ 0.266	0.01972 $\pm$ 0.00752	0.001868 $\pm$ 0.002180	0.26	98.0	24.2	21.8	455.60 $\pm$ 20.72
BB7406	1.05	26.589 $\pm$ 0.434	0.02736 $\pm$ 0.01682	0.000606 $\pm$ 0.004174	0.11	99.3	10.4	15.7	446.46 $\pm$ 39.13
BB7407	3.00	28.075 $\pm$ 1.393	0.03025 $\pm$ 0.07382	0.007929 $\pm$ 0.014495	0.04	91.7	3.5	14.2	436.28 $\pm$ 134.6
Inverse isochron age $\pm 2\sigma$		446.78 $\pm$ 35.41						Integrated age $\pm 2\sigma$	
$^{40}\text{Ar}/^{39}\text{Ar}$ intercept $\pm 2\sigma$		530.3 $\pm$ 2402		MSWD 0.11				Plateau age $\pm 2\sigma$	
BB7409	0.38	28.728 $\pm$ 0.265	0.00652 $\pm$ 0.01047	0.002271 $\pm$ 0.002460	0.24	97.7	28.6	66.0	470.93 $\pm$ 22.80
BB7410	0.53	27.684 $\pm$ 0.229	0.01200 $\pm$ 0.00684	0.000846 $\pm$ 0.001457	0.37	99.1	45.6	35.8	461.70 $\pm$ 14.45
BB7411	0.75	26.727 $\pm$ 0.460	0.01548 $\pm$ 0.01575	0.001498 $\pm$ 0.003317	0.15	98.3	19.0	27.8	444.56 $\pm$ 32.37
BB7413	1.05	27.716 $\pm$ 1.236	0.05362 $\pm$ 0.05281	0.000074 $\pm$ 0.014853	0.04	99.9	4.9	8.0	465.62 $\pm$ 135.1
BB7414	3.00	27.586 $\pm$ 3.149	0.01123 $\pm$ 0.12270	0.000188 $\pm$ 0.045609	0.02	99.8	1.9	38.3	463.13 $\pm$ 410.7
Inverse isochron age $\pm 2\sigma$		437.34 $\pm$ 124.53						Integrated age $\pm 2\sigma$	
$^{40}\text{Ar}/^{39}\text{Ar}$ intercept $\pm 2\sigma$		1609 $\pm$ 10315		MSWD 0.45				Plateau age $\pm 2\sigma$	

*Note:* All ages calculated relative to 28.02 Ma for the Fish Canyon tuff sanidine (Renne et al., 1998); using the decay constants of Steiger and Jäger (1977); uncertainties in Ar isotope ratios reported at 1 $\sigma$  analytical precision, uncertainties in ages reported at 2 $\sigma$  analytical precision. Corrected for  $^{37}\text{Ar}$  and  $^{39}\text{Ar}$  decay, half lives of 35.2 days and 269 years, respectively.

**SUPPLEMENTARY TABLE 3. STRATIGRAPHIC AND BIOSTRATIGRAPHIC  
REFERENCES FOR NUMBERED SECTIONS IN FIGURE 2**

Section	Section	Location	Reference(s)
1	Shadow Falls	St. Paul, MN	Anderson (1959), Thompson (1959), Templeton and Willman (1963), Sloan et al. (1987)
2	Sogn Roadcut	Goodhue County, MN	Anderson (1959), Sloan et al. (1987)
3	Rochester	Olmstead County, MN	Templeton and Willman (1963), Leslie and Bergström (1995, 2005), Simo et al. (2003)
4	Cummingsville/ Cummingsville Annex	Olmstead County, MN	Weiss (1955; 1957), Webers (1966), Sloan et al. (1987), Sweet (1987)
5	Mahoods Creek	Fillmore County, MN	Weiss (1957)
6	Sugar Creek/ Rifle Hill Quarry	Fillmore County, MN	Webers (1966), Sloan et al. (1987), Sweet (1987), Raatz and Ludvigson (1996), Simo et al. (2003)
7	Spring Grove	Houston County, MN	Weiss (1957), Sloan et al. (1987). Simo et al. (2003)
8	Locust	Winneshiek County, IA	Simo et al. (2003)
9	Connor	Winneshiek County, IA	Templeton and Willman (1963)
10	Decorah	Decorah, IA	Sloan et al. (1987)
11	Postville	Allamakee County, IA	Sloan et al. (1987)
12	Big Spring #4 drillcore	Clayton County, IA	Ludvigson et al. (2004)
13	Ion	Clayton County, IA	Templeton and Willman (1963)
14	MacGregor/ Pikes Peak	Clayton County, IA	Templeton and Willman (1963), Votaw (1971), Leslie and Bergström (2005)
15	Elkader A1 drillcore	Clayton County, IA	Ludvigson et al. (2004)
16	HW 52 sections/ Highway X-56/	Guttenberg, IA	Anderson (1959), Templeton and Willman (1963), Clark (1971), Delgado (1983), Sloan et al. (1987), Simo et al. (2003)
17	Spechts Ferry/ Dickeyville	Dubuque County, IA/ Grant County, WI	Templeton and Willman (1963), Leslie and Bergström (2005)
18	Sageville Quarry/ East Dubuque	Dubuque County, IA	Templeton and Willman (1963), Willman and Kolata (1978), Delgado (1983)
19	Menominee Station/ Galena Northwest	Jo Daviess County, IL	Willman and Kolata (1978)
20	Galena Type Area	Jo Daviess County, IL	Templeton and Willman (1963), Willman and Kolata (1978)
21	Wise Lake	Jo Daviess County, IL	Templeton and Willman (1963) Willman and Kolata (1978)
22	Maquoketa Formation	Iowa	Parker et al. (1959), Clark (1971), Witzke and Glenister, (1987), Goldman and Bergström (1997), Witzke and Ludvigson (2005)

**SUPPLEMENTARY TABLE 4. ABBREVIATIONS FOR GENUS SPECIES BINOMIALS AND TIERED INTERPOLATION AGES FOR ORDOVICIAN INDEX TAXA**

<b>Genus</b>	<b>Species</b>	<b>Abbreviation</b>	<b>Tiered Interpolation Age</b>	
<b>Midcontinent conodont zones</b>				
<i>Aphelognathus</i>	<i>shatzeri</i>	<i>A. shatzeri</i>	446.250	Ma
<i>Aphelognathus</i>	<i>divergens</i>	<i>A. divergens</i>	449.981	Ma
<i>Aphelognathus</i>	<i>grandis</i>	<i>A. grandis</i>	452.039	Ma
<i>Oulodus</i>	<i>robustus</i>	<i>O. ro.</i>	452.262	Ma
<i>Oulodus</i>	<i>velicuspis</i>		452.585	Ma
<i>Belodina</i>	<i>confluens</i>	<i>B. con.</i>	453.918	Ma
<i>Plectodina</i>	<i>tenuis</i>	<i>P. tenuis</i>	455.403	Ma
<i>Polyplacognathus</i>	<i>ramosus</i>	<i>P. ramosus (LAD)</i>	453.708	Ma
<i>Phragmodus</i>	<i>undatus</i>	<i>P. undatus</i>	456.041	Ma
<i>Belodina</i>	<i>compressa</i>	<i>B. co.</i>	456.080	Ma
<i>Erismodus</i>	<i>quadridactylus</i>	<i>E. qua.</i>	457.251	Ma
<i>Plectodina</i>	<i>aculeata</i>	<i>P. aculeata</i>	460.002	Ma
<i>Polyplacognathus</i>	<i>friendsvillensis</i>	<i>P. friends.</i>	461.253	Ma
<i>Histiodella</i>	<i>holodentata</i>	<i>H. holod.</i>	462.110	Ma
<i>Histiodella</i>	<i>sinuosa</i>	<i>H. sinuosa</i>	468.803	Ma
<i>Histiodella</i>	<i>altifrons</i>	<i>H. altifrons</i>	471.216	Ma
<i>Tripodus</i>	<i>laevis</i>	<i>T. laevis</i>	473.539	Ma
<i>Tripodus</i>	<i>combsi</i>	<i>T. combsi</i>	473.539	Ma
<i>Reutterodus</i>	<i>andinus</i>	<i>R. andinus</i>	475.499	Ma
<i>Oepikodus</i>	<i>communis</i>	<i>O. communis</i>	482.232	Ma
<i>Diaphorodus</i>	<i>deltatus</i>	<i>D. del.</i>	483.628	Ma
<i>Macrodonus</i>	<i>dianae</i>	<i>M. dia.</i>	483.946	Ma
Low Diversity Interval		Low di. in.	484.269	Ma
<i>Glyptoconus</i>	<i>quadruplicatus</i>	<i>G. qu.</i>	484.385	Ma
<i>Rossodus</i>	<i>manitouensis</i>	<i>R. ma.</i>	485.346	Ma
<i>Cordylodus</i>	<i>angulatus</i>	<i>C. angulatus</i>	485.471	Ma
<i>Cordylodus</i>	<i>lindstromi</i>	<i>C. lindstromi</i>	487.752	Ma
<b>North Atlantic conodont Zones</b>				
<i>Amorphognathus</i>	<i>ordovicicus</i>	<i>A. ordovicicus</i>	451.886	Ma
<i>Amorphognathus</i>	<i>superbus</i>	<i>A. superbus</i>	453.755	Ma
<i>Amorphognathus</i>	<i>tvaerensis</i>	<i>A. tvaerensis</i>	458.536	Ma
<i>Pygodus</i>	<i>anserinus</i>	<i>P. anserinus</i>	459.641	Ma
<i>Pygodus</i>	<i>serrus</i>	<i>P. serrus</i>	461.461	Ma
<i>Eoplacognathus</i>	<i>suecicus</i>	<i>E. suecicus</i>	462.534	Ma
<i>Eoplacognathus</i>	<i>variabilis</i>	<i>E. variabilis</i>	467.305	Ma
<i>Microzarkodina</i>	<i>parva</i>	<i>M. parva</i>	468.018	Ma
<i>Paroistodus</i>	<i>originalis</i>	<i>P. originalis</i>	470.837	Ma
<i>Baltoniodus</i>	<i>navis</i>	<i>B. nav.</i>	471.509	Ma
<i>Baltoniodus</i>	<i>triangularis</i>	<i>B. tri.</i>	471.735	Ma
<i>Oepikodus</i>	<i>evae</i>	<i>O. evae</i>	475.499	Ma
<i>Prioniodus</i>	<i>elegans</i>	<i>P. elegans</i>	483.886	Ma
<i>Paroistodus</i>	<i>proteus</i>	<i>P. proteus</i>	484.097	Ma
<i>Paltodus</i>	<i>deltifer</i>	<i>P. deltifer</i>	485.346	Ma
<i>Iapetognathus</i>	<i>fluctivagus</i>	<i>I. fluctivagus</i>	486.200	Ma

SUPPLEMENTARY TABLE 4. ABBREVIATIONS FOR GENUS SPECIES BINOMIALS AND TIERED INTERPOLATION AGES FOR ORDOVICIAN INDEX TAXA

Australasian substage	Genus	Species	Tiered Interpolation Age	
Basal Sil.	<i>Akidograptus</i>	<i>ascensus</i>	443.004	Ma
Bo5	<i>Normalograptus</i>	<i>persculptus</i>	443.678	Ma
Bo4	<i>Normalogr.</i>	<i>extraordinarius</i>	444.184	Ma
Bo3	<i>Paraorhograptus</i>	<i>pacificus</i>	446.549	Ma
Bo2	<i>pre-pacificus</i>	<i>zone</i>	450.149	Ma
Bo1	<i>Climacograptus</i>	<i>uncinatus</i>	451.658	Ma
Ea4	<i>Dicellograptus</i>	<i>gravis</i>	452.262	Ma
Ea3	<i>Dicranograptus</i>	<i>kirki</i>	452.654	Ma
Ea2	<i>Diplacanthograptus</i>	<i>spiniferus</i>	453.918	Ma
Ea1	<i>Diplacanthograptus</i>	<i>lanceolatus</i>	455.447	Ma
Gi2	<i>Orthograptus</i>	<i>calcaratus</i>	456.212	Ma
Gi1	<i>Nemagraptus</i>	<i>gracilis</i>	459.466	Ma
Da4	<i>Archiclimacograptus</i>	<i>riddellensis</i>	460.772	Ma
Da2	<i>Undulograptus</i>	<i>intersitus</i>	466.948	Ma
Da1	<i>Undulograptus</i>	<i>austrodentatus</i>	468.018	Ma
Ya2	<i>Cardiograptus</i>	<i>morsus</i>	468.757	Ma
Ya1	<i>Oncograptus</i>	<i>upsilon</i>	470.025	Ma
Ca4	<i>Isograptus</i>	<i>victoriae maximodivergens</i>	470.742	Ma
Ca3	<i>Isograptus</i>	<i>victoriae maximus</i>	471.216	Ma
Ca2	<i>Isograptus</i>	<i>victoriae victoriae</i>	471.735	Ma
Ca1	<i>Isograptus</i>	<i>victoriae lunatus</i>	473.539	Ma
Ch2	<i>Isograptus</i>	<i>primulus</i>	474.829	Ma
Ch1	<i>Didymograptellus</i>	<i>protobifidus</i>	475.287	Ma
Be4	<i>Pendeograptus</i>	<i>fruticosus 3</i>	475.456	Ma
Be3	<i>Pendeograptus</i>	<i>fruticosus 3 &amp; 4</i>	475.569	Ma
Be2	<i>Pendeograptus</i>	<i>fruticosus 4</i>	476.612	Ma
Be1	<i>Pendeograptus</i>	<i>fruticosus 4 + Tetragraptus approximatus</i>	482.011	Ma
La3	<i>Tetragraptus</i>	<i>approximatus</i>	482.406	Ma
La2b	<i>Araneograptus</i>	<i>murrayi</i>	483.628	Ma
La2a	<i>Aorograptus</i>	<i>victoriae</i>	484.146	Ma
La1b	<i>Psigraptus</i>		484.885	Ma
La1a	<i>Rhabdinopora scitulum &amp; Anisograptus</i>		485.389	Ma
pLa	<i>Rhabdinopora</i>	<i>flabelliformis flabelliformis</i>	485.882	Ma
Basal Ord.	<i>Rhabdinopora</i>	<i>flabelliformis parabola</i>	486.200	Ma

Note: Tiered interpolation ages calculated from radioisotopic ages in Table 2. Uncertainties for individual ages (not shown) can be determined via quadratic propagation of nearest radioisotopic ages and ash-stratigraphic and biostratigraphic uncertainties. Ord. and Sil. refer to the Ordovician and Silurian periods, respectively.

## References Cited

- Anderson, H.W., Jr., 1959. The conodont fauna of the lower part of the Decorah Shale in the Upper Mississippi Valley. M.S. Thesis, University of Minnesota, Minneapolis, 32 p.
- Brannon, J.C., Podosek, F.A., McLimans, R.K., 1992. Alleghenian age of the upper Mississippi valley zinc-lead deposit determined by Rb-Sr dating of sphalerite. *Nature*, 356, 509-511.
- Choi, Y.S., Simo, J.A., Saylor, B.Z., 1999. Sedimentologic and sequence stratigraphic interpretation of mixed carbonate-siliciclastic ramp, mid-continent epeiric sea, middle to upper Ordovician Decorah and Galena Formations, Wisconsin, in: Harris, P.M., Saller, A.H., Simo, J.A. (Eds.), *Carbonate Sequence Stratigraphy: Applications to Reservoirs, Outcrops and Models*. Special Publication 63, SEPM (Society for Sedimentary Geology), pp. 275–289.
- Clark, D.L. (Ed.), 1971. *Conodonts and Biostratigraphy of the Wisconsin Paleozoic*, Information Circular 19, University of Wisconsin-Madison Extension, 151 p.
- Delgado, D.J., 1983. Road log, Dubuque to Decorah, 1 October 1983, in: Delgado, D.J. (Ed.), *Guidebook for the 13th Annual Field Conference*. Great Lakes Section SEPM, pp. R1-R38.
- Goldman, D., and Bergström, S.M., 1997. Late Ordovician graptolites from the North American midcontinent. *Palaeontology*, 40, 965-1010.
- Leslie, S.A., and Bergström, S.M., 1995. Revision of the North American late Middle Ordovician standard stage classification and timing of the Trenton transgression based on K-bentonite correlation, in Cooper, J.D., Droser, M.L., Finney, S.C. (Eds.), *Ordovician Odyssey: Short Papers for the Seventh International Symposium on the Ordovician System*, Las Vegas, NV. Pacific Section Society for Sedimentary Geology (SEPM), pp. 49-54.
- Leslie, S.A., Bergström, S.M., 2005. Conodont biostratigraphy across the Turinian-Chatfieldian stage transition (Late Ordovician, Mohawkian) in the upper Mississippi valley, in: Ludvigson, G.A., Bunker, B.J. (Eds.), *Facets of the Ordovician Geology of the Upper Mississippi Valley Region*. Guidebook No. 24, Iowa Geological Survey, pp. 30-33.
- Ludvigson, G.A., Witzke, B.J., González, L.A., Carpenter, S.J., Schneider, C.L., Hasiuk, F., 2004. Late Ordovician (Turinian-Chatfieldian) carbon isotope excursions and their stratigraphic and paleoceanographic significance. *Palaeogeography Palaeoclimatology Palaeoecology*, 210, 187-214.
- Parker, M.C., Dorheim, F.H., Campbell, R.B., 1959. Resolving discrepancies between surface and subsurface studies of the Maquoketa Formation of northeast Iowa. *Proceedings of the Iowa Academy of Science*, 66, 248-256.
- Raatz, W.D., Ludvigson, G.A., 1996. Depositional environments and sequence stratigraphy of Upper Ordovician epicontinental deep water deposits, eastern Iowa and southern Minnesota, in: Witzke, B.J., Ludvigson, G.A., Day, J. (Eds.), *Paleozoic Sequence Stratigraphy: Views from the North American Craton*. Special Paper 306, Geological Society of America, pp. 143-159.
- Renne, P.R., Swisher, C.C., Deino, A.L., Karner, D.B., Owens, T.L., DePaolo, D.J., 1998. Intercalibration of standards, absolute ages and uncertainties in  $^{40}\text{Ar}/^{39}\text{Ar}$  dating. *Chemical Geology*, 145, 117-152.
- Simo, J.A., Emerson, N.R., Byers, C.W., Ludvigson, G.A., 2003. Anatomy of an embayment in an Ordovician epeiric sea, Upper Mississippi Valley, USA. *Geology*, 31, 545-548.
- Sloan, R.E., Kolata, D.R., Witzke, B.J., Ludvigson, G.A., 1987. Description of major outcrops in Minnesota and Iowa, in: Sloan, R.E. (Ed.), *Middle and Late Ordovician lithostratigraphy and biostratigraphy of the Upper Mississippi Valley*. Report of Investigations 35, Minnesota Geological Survey, pp. 197-231.
- Steiger, R.H., Jäger, E., 1977. Subcommission on geochronology: Convention on the use of decay constants in geo- and cosmochronology. *Earth and Planetary Science Letters*, 36, 359-362.
- Sweet, W.C., 1987. Distribution and significance of conodonts in Middle and Upper Ordovician strata of the upper Mississippi valley region, in: Sloan, R.E. (Ed.), *Middle and Late Ordovician lithostratigraphy and biostratigraphy of the Upper Mississippi Valley*. Report of Investigations 35, Minnesota Geological Survey, p. 167-172.
- Templeton, J.S., Willman, H.B., 1963. *Champlainian Series (Middle Ordovician) in Illinois*. Bulletin 89, Illinois State Geological Survey, 91 p.
- Thompson, W.H., Jr., 1959. *Conodonts of the Platteville Formation of southeastern Minnesota*. M.S. Thesis, University of Minnesota, Minneapolis, 168 p.
- Votaw, R.B., 1971. *Conodont biostratigraphy of the Black River Group (Middle Ordovician) and equivalent rocks of the eastern midcontinent, North America*. Ph.D. Thesis, The Ohio State University, Columbus, 170 p.
- Webers, G.F., 1966. The Middle and Upper Ordovician conodont faunas of Minnesota. Special Publication SP-4, Minnesota Geological Survey, 123 p.
- Weiss, M.P., 1955. Some Ordovician brachiopods from Minnesota and their stratigraphic relations. *Journal of Paleontology*, 29, 759-774.
- Weiss, M.P., 1957. Upper Middle Ordovician stratigraphy of Fillmore County, Minnesota. *Geological Society of America Bulletin*, 68, 1027-1062.
- Willman, H.B., Kolata, D.R., 1978. The Platteville and Galena Groups in northern Illinois. Circular 502, Illinois State Geological Survey, 75 p.
- Witzke, B.J., Glenister, A.T., 1987. Upper Ordovician Maquoketa Formation in the Graf area, eastern Iowa, in: Biggs, D.L. (Ed.), *North-Central Section of the Geological Society of America Centennial Field Guide 3*. Geological Society of America, p. 103-108.
- Witzke, B.J., and Ludvigson, G.A., 2005. The Ordovician Galena Group in Iowa and its regional stratigraphic relationships, in: Ludvigson, G.A., Bunker, B.J. (Eds.), *Facets of the Ordovician Geology of the Upper Mississippi Valley Region*. Guidebook No. 24, Iowa Geological Survey, p. 3-22.